A luminous X-ray outburst from an intermediate-mass black hole in an off-centre star cluster

Dacheng Lin, Jay Strader, Eleazar R. Carrasco, Dany Page, Aaron J. Romanowsky, Jeroen Homan, Jimmy A. Irwin, Ronald A. Remillard, Olivier Godet, Natalie A. Webb, et al.

LETTER

A luminous X-ray outburst from an intermediate-mass black hole in an off-centre star cluster

Dacheng Lin[1], Jay Strader[2], Eleazar R. Carrasco[3], Dany Page[4], Aaron J. Romanowsky[5,6], Jeroen Homan[7,8], Jimmy A. Irwin[9], Ronald A. Remillard[10], Olivier Godet[11], Natalie A. Webb[11], Holger Baumgardt[12], Rudy Wijnands[13], Didier Barret[11], Pierre-Alain Duc[14], Jean P. Brodie[6], Stephen D. J. Gwyn[15]

[1]Space Science Center, University of New Hampshire, Durham, NH 03824, USA [2]Center for Data Intensive and Time Domain Astronomy, Department of Physics and Astronomy, Michigan State University, 567 Wilson Road, East Lansing, MI 48824, USA [3]Gemini Observatory/AURA, Southern Operations Center, Casilla 603, La Serena, Chile [4]Instituto de Astronomía, Universidad Nacional Autónoma de México, México C.D.M.X., 04510, México [5]Department of Physics and Astronomy, San José State University, One Washington Square, San José, CA 95192, USA [6]University of California Observatories, 1156 High Street, Santa Cruz, CA 95064, USA [7]Eureka Scientific, Inc., 2452 Delmer Street, Oakland, California 94602, USA [8]SRON, Netherlands Institute for Space Research, Sorbonnelaan 2, 3584 CA Utrecht, The Netherlands [9]Department of Physics and Astronomy, University of Alabama, Box 870324, Tuscaloosa, AL 35487, USA [10]MIT Kavli Institute for Astrophysics and Space Research, MIT, 70 Vassar Street, Cambridge, MA 02139-4307, USA [11]IRAP, Universit de Toulouse, CNRS, UPS, CNES, Toulouse, France [12]School of Mathematics and Physics, University of Queensland, St Lucia, Queensland 4068, Australia [13]Anton Pannekoek Institute for Astronomy, University of Amsterdam, Postbus 94249, 1090 GE Amsterdam, The Netherlands [14]Université de Strasbourg, CNRS, Observatoire astronomique de Strasbourg, UMR 7550, F-67000 Strasbourg, France [15]Canadian Astronomy Data Centre, Herzberg Institute of Astrophysics, 5071 West Saanich Road, Victoria, British Columbia, V9E 2E7, Canada

A unique signature for the presence of massive black holes in very dense stellar regions is occasional giant-amplitude outbursts of multiwavelength radiation from tidal disruption and subsequent accretion of stars that make a close approach to the black holes[1]. Previous strong tidal disruption event (TDE) candidates were all associated with the centers of largely isolated galaxies[2–6]. Here we report the discovery of a luminous X-ray outburst from a massive star cluster at a projected distance of 12.5 kpc from the center of a large lenticular galaxy. The luminosity peaked at $\sim 10^{43}$ erg s^{-1} and decayed systematically over 10 years, approximately following a trend that supports the identification of the event as a TDE. The X-ray spectra were all very soft, with emission confined to be $\lesssim 3.0$ keV, and could be described with a standard thermal disk. The disk cooled significantly as the luminosity decreased, a key thermal-state signature often observed in accreting stellar-mass black holes. This thermal-state signature, coupled with very high luminosities, ultrasoft X-ray spectra and the characteristic power-law evolution of the light curve, provides strong evidence that the source contains an intermediate-mass black hole (IMBH) with a mass of a few ten thousand solar mass. This event demonstrates that one of the most effective means to detect IMBHs is through X-ray flares from TDEs in star clusters.

We discovered the X-ray source 3XMM J215022.4−055108 (referred to as J2150−0551 hereafter) in our project of searching for TDEs from the *XMM-Newton* X-ray source catalog. The source was serendipitously detected in 2006–2009 in two *XMM-Newton* observations and one *Chandra* observation of a field in the second Canadian Network for Observational Cosmology Field Galaxy Redshift Survey[7]. It was still detected, but with much lower X-ray fluxes, in our follow-up *Swift* observation in 2014 and *Chandra* observation in 2016. Figure 1 shows the *Hubble Space Telescope* (*HST*) ACS F775W image around the field of J2150−0551 taken in 2003. The source lies at an angular offset of 11.6 arcsec from the center of the barred lenticular galaxy 6dFGS gJ215022.2-055059 (referred to as Gal1 hereafter) and is spatially coincident with a faint optical object. Gal1 is at a redshift of $z = 0.055$ or a luminosity distance of $D_L = 247$ Mpc (for $H_0 = 70$ km s^{-1} Mpc^{-1}, $\Omega_{\rm M} = 0.3$, $\Omega_\Lambda = 0.7$). The chance probability for J2150−0551 to be within 11.6 arcsec from the center of a bright galaxy like Gal1 is very small (0.01%, see *SI*), strongly supporting the association of J2150−0551 with Gal1.

The fits to the X-ray spectra with a standard thermal thin disk are shown in the lower panels in Figure 2 (see also Table 1), and the inferred long-term evolution of the bolometric disk luminosity is plotted in the upper panel. The dependence of the bolometric disk luminosity on the apparent maximum disk temperature is plotted in Figure 3. The most striking feature is that the disk luminosity approximately scales with the temperature as $L \propto T^4$ (i.e., a constant inner disk radius, the solid line in the figure), as often observed in accreting stellar-mass black holes in the thermal state, during which a standard thermal thin disk dominates the X-ray emission[8,9]. The disk cooled significantly, with the disk temperature decreasing from 0.28 to 0.14 keV, as the disk luminosity decreased by one order of magnitude from 1.1×10^{43} to 1.1×10^{42} erg s^{-1} within 10 years. Therefore we have conclusive evidence that most observations were in the thermal state. The brightest observation (X1 hereafter), taken by *XMM-Newton* in 2006, shows a significant deviation from the $L \propto T^4$ relation traced out by the other observations. The X-ray spectrum in this observation seems to have a disk temperature profile more characteristic of a super-Eddington accretion state (see *SI*), in which the radiation pressure is stronger than the gravitational force in the inner disk. Based on fits with a more physical disk model *optxagnf*[10] to the thermal-state observations, we infer an IMBH in J2150−0551, with a mass between 5×10^4 and 10^5 $M_\odot$, depending on the spin parameter assumed (see *SI*).

An optical flare was detected between May and November in 2005, before the X-ray detections (Figure 2), with the source appearing significantly bluer and brighter — by $\sim$0.8 mag in the g' band — than in August 2000. Enhanced optical emission was not observed in the *HST* image in September 2003 (see *SI*). Therefore we constrain the outburst start time of J2150−0551 to be between September 2003 and May 2005.

The fit to the quiescent photometry of the optical counterpart to

J2150−0551 in 2000–2003 with a single stellar population model[11] implies a star cluster with a stellar mass $\sim 10^7\ M_\odot$ and a bolometric stellar luminosity of $\sim 10^7\ L_\odot$ (see *SI*). The optical source is spatially unresolved in the *HST* F775W image, with the half-light radius estimated to be $\lesssim 20$ pc (see *SI*). All these properties suggest a massive star cluster. It could be a very massive globular cluster[12] or more likely a remnant nucleus of a tidally stripped dwarf galaxy in a minor merger[13,14], given that the galaxy might be in an epoch of frequent minor mergers — there seems to be a minor merger of a satellite galaxy with Gal1 near J2150−0551 (Figure 1).

The standard TDE theory[1,15] predicts the mass accretion rate to decay with the time t after the stellar disruption as $t^{-5/3}$. A simple TDE model for the luminosity evolution of J2150−0551 is shown as a solid line in the upper panel in Figure 2, indicating that the luminosity of the source decayed approximately as $t^{-5/3}$. The time when the star was disrupted is inferred to be around mid October 2003, which is consistent with the constraint on the outburst start time from the optical variability. Prior to the observation X1, the mass accretion rate was most likely super-Eddington, in which case the luminosity would be maintained at around the Eddington limit owing to the effects of photon trapping and mass outflows[16]. Therefore, we assume a constant luminosity before X1. This Eddington-limited plateau is supported by the non-detection of the source in an *XMM-Newton* slew observation in 2004 and also by the low variability of the optical flux in the flaring phase in 2005 (see *SI*). Further assuming that the rise was fast and occurred one month after the disruption[17], we estimate the total energy released until the last *Chandra* observation to be 8.9×10^{50} ergs, and the corresponding mass accreted into the black hole was $0.061(0.1/\eta)$ $M_\odot$, where η is the efficiency in converting rest mass into radiated energy in the sub-Eddington accretion phase. These values of released energy and accreted mass are typical of other known TDEs[18–20], but few TDEs[6] are known to sustain super-Eddington accretion rates for long periods, as J2150−0551 likely did.

The optical counterpart to J2150−0551 is very faint, and we observed no clear emission lines or absorption features in our recent Gemini observation. Although we cannot determine its redshift through spectroscopy, we can securely rule out alternative explanations for the source based on its unique X-ray spectral properties (see *SI*). Only a neutron star in a low-mass X-ray binary thermally cooling right after the crust being heated in a large accretion outburst could mimic the X-ray spectral evolution observed in J2150−0551. However, this explanation is strongly disfavored, given the absence of a large accretion outburst in the light curve from the All-sky Monitor onboard the *RXTE* (see *SI*).

Because J2150−0551 was discovered through our systematic search over the *XMM-Newton* X-ray source catalog, we can estimate the rate of off-center TDEs like J2150−0551 and find it to be $\sim 10^{-8}$ Mpc^{-3} yr^{-1} (see *SI*). The TDE rate for black holes with masses of a few $10^4\ M_\odot$ in star clusters was predicted[21–23] to be between 10^{-5}–10^{-3} yr^{-1} per black hole. Then our discovery of J2150−0551 implies a significant number of off-center IMBHs with masses of a few $10^4\ M_\odot$ in the local Universe, with a space density between $\sim 10^{-5}$–10^{-3} Mpc^{-3}.

Our study of the *XMM-Newton* X-ray source catalog also led to the discovery of a possible TDE associated with the nucleus of an isolated dwarf galaxy[24] that could contain a black hole with a mass of 10^4–$10^5\ M_\odot$. The nuclei of dwarf galaxies probably have similar stellar densities and thus similar TDE rates as seen in off-center very massive ($\sim 10^7\ M_\odot$) star clusters[25]. Then our discovery of similar numbers of centered and off-center TDEs for small black holes with masses of a few $10^4\ M_\odot$ could imply similar numbers of centered and off-center black holes in this mass range[26].

A large majority of IMBHs might be electromagnetically invisible if they preferentially form in dense star clusters, which tend to be devoid of gas[27]. Indeed, a wide variety of searching strategies have found very few strong IMBH candidates with masses of 10^2–$10^5\ M_\odot$. ESO 243-49 HLX-1, which also lies in a lenticular galaxy, was the only one clearly showing very similar X-ray spectral evolution — especially the $L \propto T^4$ scaling relation for the disk — to that observed in accreting stellar-mass black holes, except that ESO 243-49 HLX-1 had three orders of magnitude higher luminosities and much lower disk temperatures as expected for an IMBH[28–30] with a mass of $\sim 10^4\ M_\odot$. J2150−0551 and ESO 243−49 HLX-1 followed a very similar L—T^4 scaling relation (Figure 3), implying that they host black holes with very similar masses (see *SI*). One main difference is that ESO 243−49 HLX-1 showed frequent X-ray outbursts and was unlikely to be due to a single disruption of a star. Our event demonstrates that IMBHs off-center from their primary host galaxies may generate TDEs if they reside in dense star clusters. Because TDEs of IMBHs are expected to easily reach the maximum luminosity, i.e., the Eddington limit[17], as seen in our event, they provide a powerful way to detect super-Eddington accreting IMBHs to a large distance.

1. Rees, M. J. Tidal disruption of stars by black holes of 10 to the 6th–10 to the 8th solar masses in nearby galaxies. *Nature* **333**, 523–528 (1988).
2. Komossa, S. & Bade, N. The giant X-ray outbursts in NGC 5905 and IC 3599:() hfill Follow-up observations and outburst scenarios. *Astron. Astrophys.* **343**, 775–787 (1999). arXiv:astro-ph/9901141.
3. Gezari, S. *et al.* An ultraviolet-optical flare from the tidal disruption of a helium-rich stellar core. *Nature* **485**, 217–220 (2012). 1205.0252.
4. Zauderer, B. A. *et al.* Radio Monitoring of the Tidal Disruption Event Swift J164449.3+573451. II. The Relativistic Jet Shuts Off and a Transition to Forward Shock X-Ray/Radio Emission. *Astrophys. J.* **767**, 152 (2013). 1212.1173.
5. Miller, J. M. *et al.* Flows of X-ray gas reveal the disruption of a star by a massive black hole. *Nature* **526**, 542–545 (2015). 1510.06348.
6. Lin, D. *et al.* A likely decade-long sustained tidal disruption event. *Nature Astronomy* **1**, 0033 (2017). 1702.00792.
7. Connelly, J. L. *et al.* Exploring the Diversity of Groups at 0.1¡z¡0.8 with X-Ray and Optically Selected Samples. *Astrophys. J.* **756**, 139 (2012). 1208.0344.
8. Remillard, R. A. & McClintock, J. E. X-Ray Properties of Black-Hole Binaries. *Annu. Rev. Astron. Astrophys.* **44**, 49–92 (2006). astro-ph/0606352.
9. Done, C., Gierliński, M. & Kubota, A. Modelling the behaviour of accretion flows in X-ray binaries. Everything you always wanted to know about accretion but were afraid to ask. *Astron. Astrophys. Rev* **15**, 1–66 (2007). 0708.0148.
10. Done, C., Davis, S. W., Jin, C., Blaes, O. & Ward, M. Intrinsic disc emission and the soft X-ray excess in active galactic nuclei. *Mon. Not. R. Astron. Soc.* **420**, 1848–1860 (2012). 1107.5429.
11. Maraston, C. Evolutionary population synthesis: models, analysis of the ingredients and application to high-z galaxies. *Mon. Not. R. Astron. Soc.* **362**, 799–825 (2005). astro-ph/0410207.
12. Mieske, S., Hilker, M. & Misgeld, I. The specific frequencies of ultra-compact dwarf galaxies. *Astron. Astrophys.* **537**, A3 (2012). 1112.4475.
13. Drinkwater, M. J. *et al.* A class of compact dwarf galaxies from disruptive processes in galaxy clusters. *Nature* **423**, 519–521 (2003). astro-ph/0306026.
14. Pfeffer, J. & Baumgardt, H. Ultra-compact dwarf galaxy formation by tidal stripping of nucleated dwarf galaxies. *Mon. Not. R. Astron. Soc.* **433**, 1997–2005 (2013). 1305.3656.
15. Phinney, E. S. Manifestations of a Massive Black Hole in the Galactic Center. In Morris, M. (ed.) *The Center of the Galaxy*, vol. 136 of *IAU Symposium*, 543 (1989).
16. Krolik, J. H. & Piran, T. Jets from Tidal Disruptions of Stars by Black Holes. *Astrophys. J.* **749**, 92 (2012). 1111.2802.
17. Guillochon, J. & Ramirez-Ruiz, E. A Dark Year for Tidal Disruption Events. *Astrophys. J.* **809**, 166 (2015). 1501.05306.
18. Li, L.-X., Narayan, R. & Menou, K. The Giant X-Ray Flare of NGC 5905: Tidal Disruption of a Star, a Brown Dwarf, or a Planet? *Astrophys. J.* **576**, 753–761 (2002). astro-ph/0203191.

19. Komossa, S. *et al.* A Huge Drop in the X-Ray Luminosity of the Nonactive Galaxy RX J1242.6-1119A, and the First Postflare Spectrum: Testing the Tidal Disruption Scenario. *Astrophys. J.* **603**, L17–L20 (2004). arXiv:astro-ph/0402468.
20. van Velzen, S. *et al.* A radio jet from the optical and x-ray bright stellar tidal disruption flare ASASSN-14li. *Science* **351**, 62–65 (2016). 1511.08803.
21. Baumgardt, H., Makino, J. & Ebisuzaki, T. Massive Black Holes in Star Clusters. II. Realistic Cluster Models. *Astrophys. J.* **613**, 1143–1156 (2004). astro-ph/0406231.
22. Brockamp, M., Baumgardt, H. & Kroupa, P. Tidal disruption rate of stars by supermassive black holes obtained by direct N-body simulations. *Mon. Not. R. Astron. Soc.* **418**, 1308–1324 (2011). 1108.2270.
23. Stone, N. C. & Metzger, B. D. Rates of stellar tidal disruption as probes of the supermassive black hole mass function. *Mon. Not. R. Astron. Soc.* **455**, 859–883 (2016). 1410.7772.
24. Lin, D. *et al.* Large decay of X-ray flux in 2XMM J123103.2+110648: evidence for a tidal disruption event. *Mon. Not. R. Astron. Soc.* **468**, 783–789 (2017). 1702.06956.
25. Norris, M. A. *et al.* The AIMSS Project - I. Bridging the star cluster-galaxy divide. *Mon. Not. R. Astron. Soc.* **443**, 1151–1172 (2014). 1406.6065.
26. Seth, A. C. *et al.* A supermassive black hole in an ultra-compact dwarf galaxy. *Nature* **513**, 398–400 (2014). 1409.4769.
27. Kızıltan, B., Baumgardt, H. & Loeb, A. An intermediate-mass black hole in the centre of the globular cluster 47 Tucanae. *Nature* **542**, 203–205 (2017). 1702.02149.
28. Farrell, S. A., Webb, N. A., Barret, D., Godet, O. & Rodrigues, J. M. An intermediate-mass black hole of over 500 solar masses in the galaxy ESO243-49. *Nature* **460**, 73–75 (2009). 1001.0567.
29. Servillat, M. *et al.* X-Ray Variability and Hardness of ESO 243-49 HLX-1: Clear Evidence for Spectral State Transitions. *Astrophys. J.* **743**, 6 (2011). 1108.4405.
30. Godet, O. *et al.* Investigating Slim Disk Solutions for HLX-1 in ESO 243-49. *Astrophys. J.* **752**, 34 (2012). 1204.3461.

Acknowledgments D.L. is supported by the National Aeronautics and Space Administration through Chandra Award Number GO6-17046X issued by the Chandra X-ray Observatory Center, which is operated by the Smithsonian Astrophysical Observatory for and on behalf of the National Aeronautics Space Administration under contract NAS8-03060, and by the National Aeronautics and Space Administration ADAP grant NNX17AJ57G. A.J.R. was supported by National Science Foundation grant AST-1515084, and as a Research Corporation for Science Advancement Cottrell Scholar. J.S. acknowledges support from NSF grant AST-1514763 and a Packard Fellowship. D.P. was partially supported by the Consejo Nacional de Ciencia y Tecnologa with CB-2014-1 Grant No. 240512. NW, OG and DB acknowledge CNES for financial support to the XMM-Newton Survey Science Center activities. R.W. acknowledges support from the Netherlands Organisation for Scientific Research through a Top Grant, module 1. J. B. acknowledges support from National Science Foundation grant AST 1518294. We thank the former *Swift* PI Neil Gehrels for approving our ToO request to make an observation of J2150−0551. We thank Zachary Jennings for assistance with the Suprime-Cam data. Based on observations obtained from XMM-Newton, Chandra, Swift, HST, CFHT, Gemini, SOAR, and Subaru.

Author Contributions D.L. wrote the main manuscript and led the data analysis. E.C. helped reduce the GMOS spectra and pre-imaging. D.P. performed the MCMC simulations for NSCool. J.S. obtained the SOAR U-band image and fitted the *HST* image with ISHAPE. A.R. obtained the Subaru g'-band image. S.G. stacked the CFHT images. All authors discussed the results and commented on the manuscript.

Competing Interests The authors declare that they have no competing financial interests.

Author Information Correspondence and requests for materials should be addressed to D.L. (dacheng.lin@unh.edu).

Table 1 | Fitting results of the high-quality X-ray spectra from J2150−0551 with an absorbed *diskbb* model. X1 and X2 are *XMM-Newton* observations, while C1 and C2 are *Chandra* observations (refer to Supplementary Table 1). All errors are at the 90% confidence level. Galactic absorption was included and fixed at $N_{\rm H,Gal} = 2.6 \times 10^{20}$ cm^{-2}. $N_{\rm H,i}$ is the absorption intrinsic to the X-ray source at redshift 0.055. It was tied together in the simultaneous fit to all spectra and then fixed at the best-fitting value when we calculated the uncertainties of other spectral parameters. The *diskbb* parameter $kT_{\rm disk}$ is the disk apparent maximum temperature, and the normalization $N_{\rm disk}$ is defined as $((R_{\rm disk}/{\rm km})/(D/10{\rm kpc}))^2 \cos\theta$, where $R_{\rm disk}$ is the apparent inner disk radius, D is the source distance, θ is the disk inclination angle. χ^2_ν is the reduced χ^2 value, and ν is the degrees of freedom. $L_{\rm abs}$ is the source rest-frame 0.32–10.6 keV (i.e., observer-frame 0.3–10 keV) luminosity, corrected for the Galactic absorption but not intrinsic absorption, and $L_{\rm unabs}$ is the source rest-frame 0.32–10.6 keV luminosity, corrected for both Galactic and intrinsic absorption. $L_{\rm disk}$ is the unabsorbed bolometric disk luminosity. We note that in the fits to X1, C1 and X2 we added a power-law component of photon index 1.8, in order to account for possible contamination from the nuclear source of Gal1; this component was found to be very weak and was not included in the luminosity calculation (see *SI*). All luminosities assume a disk inclination of 60°.

	X1	C1	X2	C2
Date	2006-05-05	2006-09-28	2009-06-07	2016-09-14
$N_{\rm H,i}$ (10^{20} cm^{-2})		$0.6^{+1.0}_{-0.6}$		
$kT_{\rm disk}$ (keV)	0.267 ± 0.005	0.279 ± 0.009	0.236 ± 0.006	0.141 ± 0.012
$N_{\rm disk}$	15.0 ± 1.4	8.6 ± 1.1	6.5 ± 0.7	$19.0^{+14.8}_{-8.9}$
$\chi^2_\nu(\nu)$	1.01(326)	1.28(101)	0.96(360)	1.70(7)
$L_{\rm abs}$ (10^{42} erg s^{-1})	$6.98^{+0.22}_{-0.21}$	$4.87^{+0.16}_{-0.15}$	$1.68^{+0.08}_{-0.08}$	$0.40^{+0.08}_{-0.08}$
$L_{\rm unabs}$ (10^{42} erg s^{-1})	$7.21^{+0.23}_{-0.22}$	$5.03^{+0.16}_{-0.16}$	$1.74^{+0.08}_{-0.08}$	$0.42^{+0.09}_{-0.08}$
$L_{\rm disk}$ (10^{42} erg s^{-1})	$10.63^{+0.35}_{-0.34}$	$7.25^{+0.30}_{-0.28}$	$2.76^{+0.14}_{-0.13}$	$1.05^{+0.32}_{-0.28}$

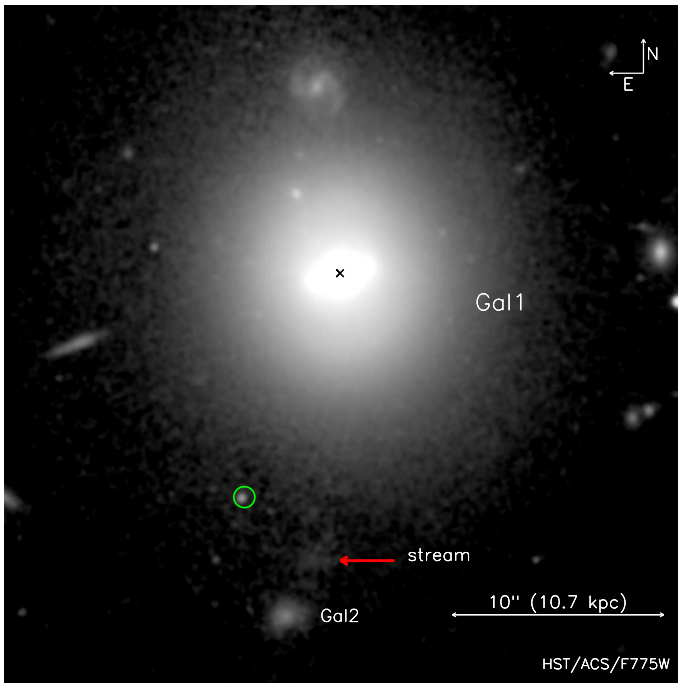

Figure 1 | The *HST*/ACS F775W imaging around the field of J2150−0551. The image was smoothed with a 2-D gaussian function of $\sigma = 0.1$ arcsec. J2150−0551 appears to be in a barred lenticular galaxy Gal1. The X-ray position of J2150−0551 from the *Chandra* observation C2 is marked with a green circle, whose radius, for clarity, is twice as large as the 99.73% X-ray positional error (0.25 arcsec). The source has a faint optical counterpart, at an offset of only 0.14 arcsec from the X-ray position. The galaxy at the bottom of the image (Gal2) could be a satellite galaxy connected with Gal1 through a tidal stream (red arrow), indicating that Gal1 is rich in minor mergers.

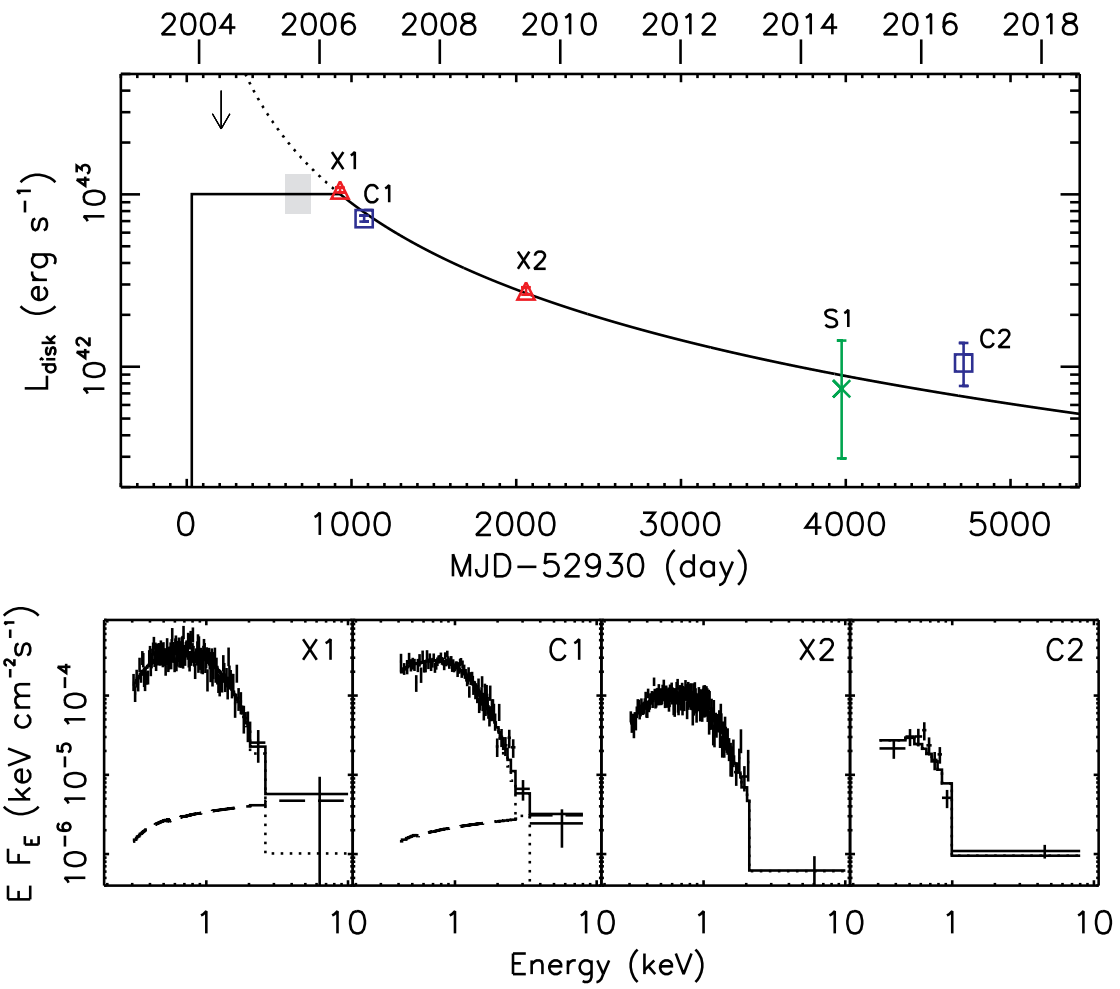

Figure 2 | The long-term luminosity and spectral evolution of J2150−0551. Upper panel: the bolometric disk luminosity curve. The *Chandra*, *XMM-Newton* and *Swift* pointed observations are shown as blue squares, red triangles and a green cross, respectively, with 90% error bars, and the arrow shows the 3σ upper limit from the *XMM-Newton* slew observation on 14 May 2004. The gray shaded region marks the time interval when the optical flare was detected in 2005. The solid line is a simple luminosity evolution model, with the luminosity following a $(t - t_{\rm D})^{-5/3}$ decline after X1 and the disruption time $t_{\rm D}$ on 18 October 2003. The rise was assumed to be fast, occurring one month after disruption, and the luminosity before X1 was assumed to be constant, given that the source was most likely in the super-Eddington accretion phase during that time. The dotted line neglects this Eddington-limited effect and predicts a luminosity a factor of 3 higher than the 3σ upper limit implied by the *XMM-Newton* slew observation. Lower panels: the standard thermal disk fits to the X-ray spectra in different observations. A power-law component (dashed line) was added in the fits to X1, C1 and X2 (inferred to be zero in this observation) to account for possible contamination of the nuclear source of Gal1 in these observations, which had relatively large point spread functions. For clarity, the spectra are rebinned to be above 2σ in each bin in the plot, and for the *XMM-Newton* observations, we only show the pn spectra. We did not fit the S1 spectrum due to its low statistics, and its luminosity was estimated based on the spectral fit to C2.

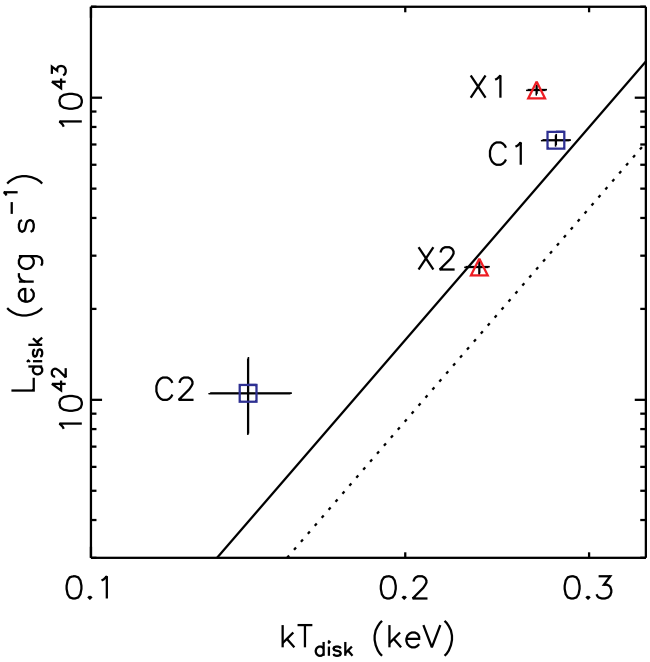

Figure 3 | The disk luminosity versus temperature derived from the fits to the X-ray spectra of J2150−0551 with the standard thermal disk model. Error bars are at the 90% confidence level. The solid line plots the $L \propto T^4$ relation with the inner disk radius being the mean value of those in C1, X2, and C2, weighted by the errors. These observations seem to follow the $L \propto T^4$ evolution (within 2.2σ), as would be expected if they were in the thermal state. X1 deviated significantly (9σ) from this evolution and can be explained if it was in the super-Eddington accretion state. The nearby dashed line plots the $L \propto T^4$ relation[29] traced out by ESO 243−49 HLX-1, suggesting that J2150−0551 and ESO 243−49 HLX-1 contain black holes of similar masses.

Method

X-ray Observations and Data Analysis

J2150−0551 was serendipitously detected in two *XMM-Newton* observations (hereafter X1 and X2) and one *Chandra* observation (hereafter C1, Supplementary Table 1) of a field in the second Canadian Network for Observational Cosmology Field Galaxy Redshift Survey[7]. X1 was taken in May 2006, and X2 in June 2009. C1 was taken in September 2006. J2150−0551 was at off-axis angles of $\sim 6'$–$8'$ in these observations. We also obtained three X-ray follow-up observations, two by *Swift* in September 2014 (hereafter S1 for their combination, Supplementary Table 1) and one by *Chandra* in September 2016.

We used SAS 16.0.0 and the calibration files of March 2017 to analyze the two *XMM-Newton* observations. The source was in the field of view (FOV) of all the three European Photon Imaging Cameras (i.e., pn, MOS1, and MOS2)[31–33] in the imaging mode in both observations. Strong background flares were seen in all cameras in both X1 and X2, and we excluded data in these intervals following the SAS thread for the filtering against high backgrounds. The exposure times of the clean data finally used are listed in Supplementary Table 1. We extracted the source spectra from all cameras using circular regions, whose radii are given in Supplementary Table 1. The background spectra were extracted from large circular regions with radii in the range of 50–100 arcsec near the source. We adopted the event selection criteria used in the pipeline[34]. We used the SAS task *rmfgen* to create the response matrix files and *arfgen* to create the point-source aperture corrected auxiliary response files. We note that there were bright columns through the source extraction region in pn in X1. These columns were excluded after the standard good event selection, resulting in a significant reduction on the source counts from pn. In both MOS1 and MOS2 cameras, a small fraction of the source counts were lost because the source was close to CCD gaps. We also performed the variability test by applying the SAS tool *ekstest* to the light curves of both observations extracted with the tool *epiclccorr*.

We note that there was no obvious pile-up for J2150−0551 in the *XMM-Newton* data because the source was not very bright. This is supported by the consistent fits obtained with the spectra from different cameras (see Supplementary Figure 2). Pile-up, if present, would affect the MOS1 and MOS2 spectra much more seriously than the pn spectra. In addition, we also created spectra using only single-pattern events, which would significantly reduce any possible pile-up, but we obtained consistent fitting results, compared with the fits to the spectra created above using all standard good events.

The C1 observation used the AXAF CCD Imaging Spectrometer (ACIS)[35], with the aimpoint and J2150−0551 falling in the front-illuminated chips I3 and I0, respectively. Our follow-up observation C2 also used the ACIS, but with the aimpoint falling in the back-illuminated chip S3 (J2150−0551 was offset from the aim point by only 9 arcsec). We reprocessed the data to apply the latest calibration (CALDB 4.7.3) using the script `chandra_repro` in the *Chandra* Interactive Analysis of Observations (CIAO) package (version 4.9). We used the CIAO task `specextract` to extract the spectra of J2150−0551 and create the corresponding response files. We extracted the source spectra using circular regions of radii 7.7 and 1.6 arcsec, enclosing 90% and 95% of the point spread function (PSF) at 1 keV, for C1 and C2, respectively. The background spectra were extracted from circular regions of radius 40 arcsec near the source in both observations. We point out that pile-up was negligible in C1 because J2150−0551 was not very bright and was at a very large off-axis angle of 8 arcmin, resulting in a very large PSF. Pile-up was not an issue in C2 either, because J2150−0551 was very faint in this observation.

There was clearly a faint source detected in C2 at the nucleus of Gal1 (hereafter Source 1). We extracted the spectra for this source from this observation as well, in the same way as we did for J2150−0551. We note that Source 1 was not clearly seen in observations X1, X2, and C1, because Source 1 was much fainter than J2150−0551 and they were hardly resolved from each other due to their large PSFs in these observations. When we fitted the spectra of J2150−0551 from X1, X2 and C1 in the *SI*, we had an extra spectral component to account for the contamination from Source 1 and found this nuclear source to be very faint, as observed in C2.

The best position of J2150−0551 can be obtained from the on-axis *Chandra* observation C2, which had the sub-arcsec resolution near the aimpoint. We carried out absolute astrometric correction and determined the statistical and systematic positional errors in the same way as we did in our previous studies[6,36]. In brief, we first carried out the X-ray source detection using the CIAO tool `wavdetect`[37], and then performed absolute astrometric correction using 25 matches of X-ray sources and optical sources from the CFH12K mosaic[38] R-band image (see below).

In the two *Swift* observations in 2014, the X-ray telescope (XRT)[39] was operated in Photon Counting mode. We analyzed the data with FTOOLS 6.20 and the calibration files of May 2017. The X-ray data were reprocessed with the task *xrtpipeline* (version 0.13.3) to update the calibration. We extracted the source and background spectra using circular regions of radii 20 and 100 arcsec, respectively.

Multi-wavelength Photometry Observations

In both *XMM-Newton* observations X1 and X2, J2150−0551 was also covered in the images of the Optical Monitor (OM)[40], which used only the *UVM2* (2310 Å) filter. The source was not detected in these images, whose 3σ detection limit was $\sim$22.0 AB mag. In both *Swift* observations in September 2014, the UV-Optical Telescope (UVOT)[41] images used the $UVW2$ (2120 Å) filter. J2150−0551 was not detected either in these images, whose 3σ detection limit was 24.3 AB mag.

J2150−0551 happened to be covered in an image from the Advanced Camera for Surveys (ACS) Wide Field Camera (WFC) on the *Hubble Space Telescope* (*HST*) on 13 September 2003 (Supplementary Table 2). As will be shown, it clearly revealed a very faint counterpart to J2150−0551. The image was composed of four 510-s exposures, but J2150−0551 was covered by only two of them because it happened to be in the CCD gap (in the north-south direction) in the other two exposures. We measured the photometry using a circular source region of radius 0.5 arcsec and an annular background region of inner radius 0.6 arcsec and outer radius 0.8 arcsec. The photometry was then corrected for the PSF loss[42].

There are also many optical/IR observations in the field of J2150−0551 by the CFH12K mosaic[38], the MegaPrime/MegaCam[43] and the WIRCam[44] on the Canada-France-Hawaii Telescope (CFHT, Supplementary Table 2). We used the calibrated images obtained in the literature[45]. They were calibrated by comparing with the SDSS photometry. These ground-based images have much larger PSFs than the *HST* image. Therefore, there is significant non-uniform stellar emission of the host galaxy at the position of J2150−0551, making the calculation of the photometry of our source in these images non-trivial. We carried out detailed fits to the profile of the host galaxy plus the counterpart to J2150−0551 in these images using GALFIT[46] in order to calculate the photometry of J2150−0551. Multiple Sérsic functions convolved with the PSF were used to fit the galaxy profile, while a PSF model was used to fit the counterpart to J2150−0551, which showed no evidence of being resolved in the *HST* image. Because the main goal was to obtain the photometry of J2150−0551, we tried to use an adequate number of Sérsic functions to ensure reasonable fits to the host galaxy emission. The exact numbers of Sérsic functions used varied with images and were in the range between five and nine.

To measure the current optical emission level, we obtained a SOAR U-band image and a Subaru g-band image of our source in

2014 (Supplementary Table 2). We also obtained a Gemini $r_{\rm G0326}$-band image, which was used to design the mask for the Gemini Multi-Object Spectrograph (GMOS)[47] observation of J2150−0551 (program id GS-2016A-Q-20). All these images were reduced and calibrated using standard procedures. The above GALFIT photometry method was also applied to these images.

The GMOS Observation

A special mask was designed for the GMOS observation of J2150−0551, Gal1, and Gal2 (see Supplementary Figure 1). To take full advantage of the multi-object spectroscopy capabilities of the instrument, other galaxies were also included in the mask design, but the analysis and scientific use of them will be presented in a separate paper. The GMOS spectroscopic data were obtained during the nights of 27 September 2016 and 4 November 2016, in dark conditions, with a good sky transparency and a median seeing between 0.45 and 0.55 arcsec. All spectra were acquired with the R400 grating centered at 5500 Å. A total exposure time of 3 hours (6×1800 seconds) was obtained for the mask. Small offsets of ∼50 Å between exposures toward the blue and red were applied to avoid the loss of any important lines present in the spectra. All objects in the mask were observed with 1 arcsec slit widths, except Gal2, which has a larger size and thus was observed with a 1.5 arcsec slit width.

The spectroscopic data were reduced with the GEMINI package version 1.3.1 inside IRAF. The science spectra, comparison lamps and spectroscopic flats were bias/overscan subtracted, trimmed and flat fielded using the spectroscopic flats. The 2-D spectra were then wavelength calibrated, corrected by S-shape distortions and sky-subtracted. Because our primary interest resided in the galaxies Gal1 and Gal2 and the optical counterpart to J2150−0551, only the spectra of these three objects were extracted to a one-dimensional format. For Gal1 and Gal2, we used a fixed aperture of 1.4 arcsec. For the optical counterpart to J2150−0551, a fixed aperture of 0.8 arcsec was used, with the background taken to be the mean of two background regions that were on different sides of the source and had the same size as the source aperture, in order to account for the effect of the Gal1 stellar emission near J2150−0551. The residual values in the wavelength solution for ∼25 points using a 5th-order Chebyshev polynomial typically yielded *rms* values of ∼0.15 Å. The final spectral resolution (FWHM, measured from the sky lines at 6300 Å) is ∼7.1 Å for Gal1 and the optical counterpart to J2150−0551 (1 arcsec slit width) and ∼8.2 Å for Gal2 (1.5 arcsec slit width). The wavelength coverage was ∼4200–8000 Å, depending on the position of the slit in the GMOS FOV. Finally, the 1D spectra were calibrated in flux using the observation of the spectrophotometric standard star LTT 1788. Because this standard star was observed on a different night (2 February 2016) and under different observing conditions, the science spectra were only relatively calibrated in flux.

We fitted the GMOS spectra with Penalized Pixel Fitting (`pPXF`) software[48], which extracts the stellar kinematics or stellar population from spectra of galaxies with the penalized pixel-fitting method. We used multi-component models comprised of single-population synthetic spectra[49], spanning a grid of 48 ages between 0.06 to 14 Gyr and 7 metallicities [M/H]={−2.32, −1.71, −1.31, −0.71, −0.40, 0.00, +0.22}. For the spectrum of the nuclear region of Gal1, we added several Gaussian lines to model the possible presence of emission lines. This spectrum is of high quality, and we incorporated a multiplicative polynomial of 10 degrees to account for possible calibration uncertainties. The spectra of Gal2 and J2150−0551 are noisy, and we did not incorporate a multiplicative polynomial in the fits. All spectra were corrected for the Galactic dust reddening[50] of $\rm E(B-V)_G = 0.03$ mag before the fits.

Numerical modeling of a cooling neutron star scenario for J2150−0551

As will shown in the *SI*, the very soft X-ray spectra of J2150−0551 approximately resemble those of thermally cooling neutron stars (NSs) in low-mass X-ray binaries (LMXBs) often detected after large outbursts due to accretion[51,52]. Cooling curves have been observed in about ten NS LMXBs[53], and they were generally explained as the cooling of the NS crust after being heated by non-equilibrium nuclear reactions during large accretion outbursts[54,55]. We need to estimate the mass accretion rate $\dot{M}$ needed to produce the hypothetically observed cooling curve of J2150−0551 and compare this $\dot{M}$ with the detection limit from the All-Sky Monitor (ASM)[56] onboard the *RXTE*, in order to check the feasibility of the cooling NS explanation for J2150−0551. We estimated $\dot{M}$ through extensive Markov chain Monte Carlo (MCMC) simulations with the code `NSCool`[57–59], using an MCMC driver inspired from the `emcee` code[60]. We used 200 "walkers" exploring simultaneously the parameter space. The parameters of the MCMC runs covered a wide range of possibilities about the structure and microphysics of the NS and the characteristics of the accretion outburst responsible for the heating of the NS prior to the four observations X1, C1, X2, and C2. We modeled the accretion phase as a step function in time with a constant $\dot{M}$, with the start time constrained to be between 14 May 2004 and 3 June 2005 and the end time to be between 7 November 2005 and 5 May 2006 (see *SI*). We explored a wide range of possible values of the NS mass ($M_{\rm NS}$=1.0–2.2 $M_\odot$) and radius ($R_{\rm NS}$=8–16 km). The cooling curve and the source distance inferred from the spectral fits depend on the NS mass and radius assumed. We first obtained the cooling curves and the source distances for a grid of 13 NS masses (step 0.1 $M_\odot$) and 9 radii (step 1 km) from the spectral fits and then interpolated them to obtain the cooling curve and source distance for any NS mass and radius of each MCMC run. In order to convert $\dot{M}$ from the MCMC to the ASM count rate, we assumed a radiative efficiency of $1-\sqrt{1-2GM_{\rm NS}/R_{\rm NS}c^2}$, where c is the speed of light and G is the gravitational constant, and adopted a bolometric correction factor of five from the ASM band pass (1.5–12 keV) to 0.2–100 keV, based on typical low-state spectra of NS LMXBs[61].

Shallow heating of the crust released at low densities (∼10^8–10^{10} g cm^{-3}), beyond the deep crustal heating, is often needed in explaining the cooling curves of many objects[58,62,63]. Therefore we also considered this possibility and added a shallow energy source, which was parametrized in terms of the amount of energy released per accreted nucleon, $Q_{\rm sh}$. Other parameters included in the MCMC were the amount of light elements in the stellar envelope, the impurity parameter that controled electron scattering for the thermal conductivity, and the extent of neutron superfluidity in the inner crust that strongly affected the specific heat.

Data availability statement The data that support the plots within this paper and other findings of this study are available from the corresponding author upon reasonable request.

31. Jansen, F. *et al.* XMM-Newton observatory. I. The spacecraft and operations. *Astron. Astrophys.* **365**, L1–L6 (2001).
32. Strüder, L. *et al.* The European Photon Imaging Camera on XMM-Newton: The pn-CCD camera. *Astron. Astrophys.* **365**, L18–L26 (2001).
33. Turner, M. J. L. *et al.* The European Photon Imaging Camera on XMM-Newton: The MOS cameras : The MOS cameras. *Astron. Astrophys.* **365**, L27–L35 (2001). `arXiv:astro-ph/0011498`.
34. Watson, M. G. *et al.* The XMM-Newton serendipitous survey. V. The Second XMM-Newton serendipitous source catalogue. *Astron. Astrophys.* **493**, 339–373 (2009). `0807.1067`.
35. Bautz, M. W. *et al.* X-ray CCD calibration for the AXAF CCD Imaging Spectrometer. In R. B. Hoover & A. B. Walker (ed.) *Society of Photo-Optical Instrumentation Engineers (SPIE) Conference Series*, vol. 3444

of *Society of Photo-Optical Instrumentation Engineers (SPIE) Conference Series*, 210–224 (1998).
36. Lin, D. *et al.* Discovery of the Candidate Off-nuclear Ultrasoft Hyperluminous X-ray Source 3XMM J141711.1+522541. *Astrophys. J.* **821**, 25 (2016). 1603.00455.
37. Freeman, P. E., Kashyap, V., Rosner, R. & Lamb, D. Q. A Wavelet-Based Algorithm for the Spatial Analysis of Poisson Data. *Astrophys. J. Suppl. Ser.* **138**, 185–218 (2002). arXiv:astro-ph/0108429.
38. Cuillandre, J.-C., Luppino, G. A., Starr, B. M. & Isani, S. Performance of the CFH12K: a 12K by 8K CCD mosaic camera for the CFHT prime focus. In Iye, M. & Moorwood, A. F. (eds.) *Optical and IR Telescope Instrumentation and Detectors*, vol. 4008 of *Society of Photo-Optical Instrumentation Engineers (SPIE) Conference Series*, 1010–1021 (2000).
39. Burrows, D. N. *et al.* The Swift X-Ray Telescope. *Space Science Reviews* **120**, 165–195 (2005). arXiv:astro-ph/0508071.
40. Mason, K. O. *et al.* The XMM-Newton optical/UV monitor telescope. *Astron. Astrophys.* **365**, L36–L44 (2001). arXiv:astro-ph/0011216.
41. Roming, P. W. A. *et al.* The Swift Ultra-Violet/Optical Telescope. *Space Science Reviews* **120**, 95–142 (2005). arXiv:astro-ph/0507413.
42. Sirianni, M. *et al.* The Photometric Performance and Calibration of the Hubble Space Telescope Advanced Camera for Surveys. *Publ. Astron. Soc. Pacif.* **117**, 1049–1112 (2005). astro-ph/0507614.
43. Boulade, O. *et al.* MegaCam: the new Canada-France-Hawaii Telescope wide-field imaging camera. In Iye, M. & Moorwood, A. F. M. (eds.) *Instrument Design and Performance for Optical/Infrared Ground-based Telescopes*, vol. 4841 of *Society of Photo-Optical Instrumentation Engineers (SPIE) Conference Series*, 72–81 (2003).
44. Puget, P. *et al.* WIRCam: the infrared wide-field camera for the Canada-France-Hawaii Telescope. In Moorwood, A. F. M. & Iye, M. (eds.) *Ground-based Instrumentation for Astronomy*, vol. 5492 of *Society of Photo-Optical Instrumentation Engineers (SPIE) Conference Series*, 978–987 (2004).
45. Balogh, M. L. *et al.* The colour of galaxies in distant groups. *Mon. Not. R. Astron. Soc.* **398**, 754–768 (2009). 0905.3401.
46. Peng, C. Y., Ho, L. C., Impey, C. D. & Rix, H.-W. Detailed Decomposition of Galaxy Images. II. Beyond Axisymmetric Models. *Astron. J.* **139**, 2097–2129 (2010). 0912.0731.
47. Hook, I. M. *et al.* The Gemini-North Multi-Object Spectrograph: Performance in Imaging, Long-Slit, and Multi-Object Spectroscopic Modes. *Publ. Astron. Soc. Pacif.* **116**, 425–440 (2004).
48. Cappellari, M. & Emsellem, E. Parametric Recovery of Line-of-Sight Velocity Distributions from Absorption-Line Spectra of Galaxies via Penalized Likelihood. *Publ. Astron. Soc. Pacif.* **116**, 138–147 (2004). astro-ph/0312201.
49. Vazdekis, A. *et al.* Evolutionary stellar population synthesis with MILES - I. The base models and a new line index system. *Mon. Not. R. Astron. Soc.* **404**, 1639–1671 (2010). 1004.4439.
50. Schlegel, D. J., Finkbeiner, D. P. & Davis, M. Maps of Dust Infrared Emission for Use in Estimation of Reddening and Cosmic Microwave Background Radiation Foregrounds. *Astrophys. J.* **500**, 525–+ (1998). arXiv:astro-ph/9710327.
51. Homan, J. *et al.* A Strongly Heated Neutron Star in the Transient Z Source MAXI J0556-332. *Astrophys. J.* **795**, 131 (2014). 1408.3276.
52. Degenaar, N., Ootes, L. S., Reynolds, M. T., Wijnands, R. & Page, D. A cold neutron star in the transient low-mass X-ray binary HETE J1900.1-2455 after 10 yr of active accretion. *Mon. Not. R. Astron. Soc.* **465**, L10–L14 (2017). 1609.07485.
53. Wijnands, R., Degenaar, N. & Page, D. Cooling of Accretion-Heated Neutron Stars. *Journal of Astrophysics and Astronomy* **38**, #49 (2017). 1709.07034.
54. Haensel, P. & Zdunik, J. L. Non-equilibrium processes in the crust of an accreting neutron star. *Astron. Astrophys.* **227**, 431–436 (1990).
55. Brown, E. F., Bildsten, L. & Rutledge, R. E. Crustal Heating and Quiescent Emission from Transiently Accreting Neutron Stars. *Astrophys. J.* **504**, L95+ (1998). arXiv:astro-ph/9807179.
56. Levine, A. M. *et al.* First Results from the All-Sky Monitor on the Rossi X-Ray Timing Explorer. *Astrophys. J.* **469**, L33 (1996). astro-ph/9608109.
57. Page, D., Lattimer, J. M., Prakash, M. & Steiner, A. W. Minimal Cooling of Neutron Stars: A New Paradigm. *Astrophys. J. Suppl. Ser.* **155**, 623–650 (2004). astro-ph/0403657.
58. Page, D. & Reddy, S. Forecasting Neutron Star Temperatures: Predictability and Variability. *Physical Review Letters* **111**, 241102 (2013). 1307.4455.
59. Page, D. NSCool: Neutron star cooling code. Astrophysics Source Code Library (2016). 1609.009.
60. Foreman-Mackey, D., Hogg, D. W., Lang, D. & Goodman, J. emcee: The MCMC Hammer. *Publ. Astron. Soc. Pacif.* **125**, 306 (2013). 1202.3665.
61. Armas Padilla, M., Degenaar, N. & Wijnands, R. The X-ray spectral properties of very-faint persistent neutron star X-ray binaries. *Mon. Not. R. Astron. Soc.* **434**, 1586–1592 (2013). 1303.6640.
62. Brown, E. F. & Cumming, A. Mapping Crustal Heating with the Cooling Light Curves of Quasi-Persistent Transients. *Astrophys. J.* **698**, 1020–1032 (2009). 0901.3115.
63. Deibel, A., Cumming, A., Brown, E. F. & Page, D. A Strong Shallow Heat Source in the Accreting Neutron Star MAXI J0556-332. *Astrophys. J.* **809**, L31 (2015). 1506.03846.

Supplementary Information

The X-ray Source Position and the Optical Counterpart

Figure 1 shows the *HST*/ACS image of the field around J2150−0551, which is marked with a green circle of radius twice as large as its 99.73% X-ray positional error (0.25 arcsec) that we obtained from C2. J2150−0551 appears to be on the outskirts of Gal1, a barred lenticular galaxy at $z = 0.05526 \pm 0.00003$ (from the pPXF fit below, $D_{\rm L} = 247$ Mpc, and the 6dF Galaxy Survey gave a consistent redshift[64]). J2150−0551 is at an angular offset of 11.6 arcsec, corresponding to 12.5 kpc, from the nucleus of Gal1. J2150−0551 is at an offset of only 0.14 arcsec (less than the 99.73% positional error) from a faint optical source at R.A.=21:50:22.498 and Decl.=−5:51:09.093. Further considering the correlated optical and X-ray variability, as will be demonstrated below, we can securely identify this optical source as the counterpart to J2150−0551. The number density of galaxies that are as bright as or brighter than Gal1 in the Two Micron All Sky Survey[65] $K_{\rm s}$ band (12.3 mag) near J2150−0551 is 3.9 deg^{-2}. Then the chance probability for J2150−0551 to be within 11.6 arcsec from the nucleus of Gal1 is very low, only 0.01%. Therefore, Gal1 is most likely the host of J2150−0551. Figure 1 shows that near J2150−0551 there appears to be a smaller galaxy (marked as "Gal2"), which could be connected with Gal1 with a stream and thus could be a satellite galaxy of Gal1. The possible stream is also seen in various ground-based images, such as the Gemini $r_{\rm G0326}$ image shown in Supplementary Figure 1. Therefore Gal1 could be rich in minor mergers.

To test whether the counterpart to J2150−0551 was resolved in the *HST* image, we used `ishape`[66]. We created an empirical PSF using several stars in the field and fitted a range of models, including both King and Sérsic functions. All fits were performed on the two individual flat-fielded images in which the source appears, rather than on the final drizzled image. For no model tested was there a significant improvement in the reduced χ^2 of the fit over a point source. While deeper data are desirable, we found no compelling evidence that the source was resolved in the available images. If the object was extended, its effective radius would be $\lesssim$0.02 arcsec, or 20 pc.

C1 also detected a faint X-ray source (Source 1) at an offset of only 0.06 arcsec from the optical center of Gal1. The offset is much smaller than the 99.73% X-ray positional error of Source 1 (0.39 arcsec or 0.42 kpc), supporting the nuclear origin for the source.

X-ray Spectral Modeling

The *XMM-Newton* and *Chandra* spectra (X1, C1, X2, and C2) of J2150−0551 are of good quality, and we fitted them in detail. The spectra were rebinned to have a minimum of 15 counts per bin in order to adopt the χ^2 statistic in the fits in XSPEC[67]. Because J2150−0551 most likely resides in the galaxy Gal1 at $z = 0.055$, we first explored this scenario by applying this redshift to all the spectral models that we tested with the convolution model *zashift* in XSPEC. Galactic absorption[68] of $N_{\rm H} = 2.64 \times 10^{20}$ cm^{-2} was included using the *tbabs* model, while absorption intrinsic to the source was modeled with *ztbabs*. The Wilm abundance table[69] was adopted. Because the X1, C1, and X2 spectra were obtained from relatively large source regions due to large PSFs in these observations, they might be very weakly contaminated by the nearby nuclear emission Source 1. The spectrum of Source 1 in C2 can be fitted with an absorbed power law (PL) of Galactic absorption (intrinsic absorption is consistent with zero) and $\Gamma_{\rm PL} = 1.8 \pm 0.5$ (the source rest-frame 0.32–10.6 keV unabsorbed luminosity was 6×10^{40} erg s^{-1}). Therefore, in our fits to the X1, C1, and X2 spectra, we had an extra absorbed PL component with $\Gamma_{\rm PL}$ fixed at 1.8 and $N_{\rm H}$ fixed at 2.64×10^{20} cm^{-2} to account for possible contamination from Source 1. The inferred contamination was found to be very weak and have negligible effects on the fitting results of J2150−0551.

All spectra of J2150−0551 were very soft, with little emission above 3 keV. The first spectral model that we tested was an absorbed PL. We obtained very high photon indices ($\Gamma_{\rm PL} \geq 4.8$) for all spectra. The fits showed clear systematic residuals (e.g., reduced χ^2 value χ^2_ν=1.26 for degrees of freedom $\nu = 325$ for X1). We next tried to fit the spectra with an absorbed single-temperature blackbody (*bbodyrad* in XSPEC). However, the fits were generally bad (e.g., χ^2_ν=1.45 for $\nu = 325$ for X1 and χ^2_ν=1.54 for $\nu = 100$ for C1), with the systematic residuals indicating that the spectra are broader than a single-temperature blackbody. We next tried an absorbed multicolor disk (*diskbb* in XSPEC) model and obtained acceptable fits with χ^2_ν in the range of 0.9–1.3 for X1, C1, and X2. The χ^2_ν value was higher for C2, but with $\nu = 6$, the probability that the spectrum was drawn from the model is modest (9%). All spectra inferred a small and consistent intrinsic column density $N_{\rm H,i}$. In the final fits, we fitted all spectra simultaneously with $N_{\rm H,i}$ tied to be the same. The fit results are given in Table 1 and are shown in Figure 2. The fit residuals are shown in Supplementary Figure 2. We note that we fixed $N_{\rm H,i}$ at the best-fitting value when we calculated the uncertainties of the other parameters. Fixing $N_{\rm H,i}$ could put tighter constraints on the disk parameters and allow us to determine the significance of the relative changes of the disk properties with the observations more accurately.

Figure 3 plots the bolometric disk luminosity $L_{\rm disk}$ versus the the apparent maximum disk temperature $kT_{\rm disk}$ from the *diskbb* fits. Remarkably, the disk luminosity overall approximately follows the $L \propto T^4$ relation (constant inner disk radius, the solid line in the figure), as observed in black hole (BH) X-ray binaries in the thermal state[8,9]. The disk cooled significantly, with $kT_{\rm disk}$ decreasing from ∼0.28 keV in X1 and C1 to 0.14 keV in C2 as $L_{\rm disk}$ decreased by an order of magnitude (see also Table 1). Especially from C1 to X2 in nearly three years, the apparent inner disk radius $R_{\rm disk}$ decreased only slightly (by 15%) at the 2.8σ confidence level, but $kT_{\rm disk}$ decreased from 0.28 keV to 0.23 keV at the 7.4σ confidence level. $R_{\rm disk}$ in C2 seemed to be larger than that in X2 by 71%, but only at the 2.5σ confidence level, while the cooling of the disk from X2 to C2 was very significant (10σ). Therefore, we conclude that the source was in the thermal state in C1, X2, and C2.

The most significant deviation from the $L \propto T^4$ relation was observed from X1 to C1. $R_{\rm disk}$ decreased by 32% at the 6σ confidence level from X1 to C1 in nearly four months, while $kT_{\rm disk}$ was consistent to within the 2σ error. One explanation for this deviation is that the inner disk reached the local Eddington limit in X1, which is brighter than C1 by 50%. In such a scenario, the cooling from advected photons and/or radiation-driven mass outflow in the inner disk is expected to be significant, resulting in a disk temperature profile with respect to the radius r to deviate from $T \propto r^{-3/4}$ for a standard thin disk[70–74]. Therefore we also tested the p-free disk model (i.e, $T \propto r^{-p}$, with p as a free parameter, *diskpbb* in XSPEC) for the three brightest spectra X1, C1, and X2. We found that the p parameter was not well constrained for all spectra. In order to provide a meaningful comparison of the p values among different spectra, we fixed p at the value of 0.75 for a standard disk for X2 and fixed $N_{\rm H,i}$ and the *diskpbb* normalization (thus the inner disk radius) at the best-fitting values obtained from the simultaneous fit to all three spectra with these two parameters tied together. The fit results are given in Supplementary Table 3. We inferred $p = 0.70 \pm 0.03$ (90% error) for C1, fairly close to the standard disk value (0.75) assumed in X2 (the difference is 3σ). The p value from X1 (0.610 ± 0.012) is significantly smaller than the standard disk value (at the 20σ confidence level). Therefore the fits with the absorbed *diskpbb* model also suggest that the inner disk reached the local Eddington limit in X1. We note that although the *diskpbb* model might describe X1 better than *diskbb*, the bolometric luminosity is better to be estimated with

diskbb because the local Eddington limit was expected to be reached only in the inner disk region and *diskpbb* could significantly overestimate emission from the outer disk region.

We used the AGN spectral model *optxagnf*[10] (in XSPEC) to roughly estimate the BH mass. The model was created assuming a disk inclination of 60°. It includes three components: a thermal disk, a low-temperature Comptonized component and a high-temperature Comptonized component. We applied only the thermal disk component of the model to the two thermal-state spectra that have the highest quality, i.e., C1 and X2. Therefore, there were only three free parameters of the model in our fits: the BH mass $M_{\rm BH}$, the spin parameter a^*, and the Eddington ratio. We fitted both spectra simultaneously, with all parameters except the Eddington ratio tied to be the same. The fits could not constrain both $M_{\rm BH}$ and a^* well simultaneously. We found that we required $a^* > 0.92$ if C1 and X2 were required to have the Eddington ratios below 1.0, thus in the thermal state. Assuming $a^* = 0.92$, we inferred $M_{\rm BH} = 5.3 \times 10^4\ M_\odot$ (Supplementary Table 3), which is likely the lower bound of the BH mass. The upper bound of the BH mass could be obtained assuming a maximally-rotating Kerr BH, and we got $M_{\rm BH} = 1.2 \times 10^5\ M_\odot$ (Supplementary Table 3). We did not use X1 to constrain the BH mass because it is less clear what Eddington ratio this observation assumed, though when the inner disk reached the local Eddington limit, the Eddington ratio might be[72] close to 1.0.

The very soft X-ray spectra of J2150−0551 resemble the emission from cooling NSs in LMXBs right after large accretion outbursts[53]. Therefore we also fitted the X-ray spectra of J2150−0551 with the NS atmosphere model *nsatmos*[75] (the other popular model *nsa*[76] gave very similar results). We first fixed the NS mass and radius to canonical values of $M_{\rm NS} = 1.4\ M_\odot$ and $R_{\rm NS} = 10$ km. The X1, C1, X2, and C2 spectra were fitted simultaneously, with the column density and the source distance tied to be the same. The fit results are shown in Supplementary Figure 3 and given in Supplementary Table 3. The fits were marginally acceptable. The fit to C2 had the highest χ^2_ν value (3.2, $\nu = 8$), showing clear systematic residuals. The χ^2 probability P_χ was rather low (0.1%). If we allowed the distance in C2 to be different from that of X1, C1, and X2, we obtained a better fit ($\chi^2_\nu = 1.9$, $\nu = 7$, $P_\chi = 6\%$, the fit quality was similar to that obtained with an absorbed *diskbb* model). The inferred distance was 2.6 times smaller than that from the joint fit of X1, C1, and X2, corresponding to a 2.5σ discrepancy. Because it does not make sense to adopt different source distances for different observations, from now on, we will concentrate on the fits with the source distance tied to be the same for all observations. The fits inferred the effective temperature measured by a distant observer $kT^\infty_{\rm nsatmos,eff}$ to decrease from 75 eV in X1 to 37 eV in C2. We note that these effective temperatures are much lower than the temperatures inferred from *blackbody* or *diskbb* fits because the NS quiescent spectrum as calculated in *nsatmos* tends to have a harder high-energy tail than a blackbody[55]. We could not effectively differentiate these various models in the spectral fits because the X-ray spectra were very soft, while we could only use energy bands above 0.3 keV and there was Galactic absorption ($N_{\rm H} = 3 \times 10^{20}$ cm^{-2}) at low energies.

We explored the dependence of the fits on the assumed NS mass (1.0–2.2 $M_\odot$) and radius (8–16 km). We found that $kT^\infty_{\rm nsatmos,eff}$ hardly changed ($\lesssim$4 eV) with the assumed NS mass and radius. Supplementary Table 3 also includes the fit results for $R_{\rm NS} = 13$ km and 16 km and $M_{\rm NS} = 1.4\ M_\odot$.

The Long-term and Short-term X-ray Variability

Figure 2 plots the long-term evolution of the bolometric disk luminosity $L_{\rm disk}$ of J2150−0551 inferred from the *diskbb* fits, adopting a distance of $D_L = 247$ Mpc and a disk inclination of 60°. The source was first detected in X1 on 5 May 2006, with $L_{\rm disk} \sim 1.1 \times 10^{43}$ erg s^{-1}. It was still bright in C1, X2 and C2, but with $L_{\rm disk}$ decreasing by factors of 1.5, 3.9, and 10.1, respectively. The source rest-frame 0.32–10.6 keV unabsorbed luminosity decreased by a factor of 17 from X1 to C2 (Table 1). The S1 observation in September 2014 had very low statistics, with only 7 counts detected (corresponding to $\sim 3\sigma$, one background count expected)) within 0.3–10 keV in the source region. Therefore we did not carry out spectral fits to S1. With 6 out of the 7 counts below 1 keV, the S1 spectrum could be as ultrasoft as C2. Therefore we estimated the luminosity of the source in S1 (as shown in Figure 2) assuming the *diskbb* fit to C2 and found a luminosity level consistent with that of C2.

We note that J2150−0551 was not detected in the *ROSAT* All-Sky Survey in 1990, whose detection limit was a factor of two lower than the flux of our source in X1. The source was covered but not detected in an *XMM-Newton* slew observation on 14 May 2004, which had an effective exposure of 3 seconds and the 3σ detection limit of 3×10^{-12} erg s^{-1} cm^{-2} (a factor of four higher than the flux in X1). The source was not detected in another *XMM-Newton* slew observation on 23 November 2015 either. This observation had an effective exposure of 10 seconds and the detection limit an order of magnitude above the source flux indicated by S1 and C2.

Supplementary Figure 4 shows the long-term monthly light curve of J2150−0551 from the ASM onboard the *RXTE* over the whole time of the mission. There was no significant detection of the source in any timescale. On the monthly basis, the 3σ upper limit when the source flux was not significantly affected by the Sun was typically $\lesssim$0.2 cts s^{-1}, corresponding to $<6 \times 10^{-11}$ erg s^{-1} cm^{-2} (1.5–12 keV). This limit is three orders of magnitude more than the peak flux of J2150−0551 in 1.5–12 keV (5×10^{-14} erg s^{-1} cm^{-2}, from X1), explaining why the ASM did not detect the soft X-ray outburst detected by *XMM-Newton* and *Chandra*.

Supplementary Figure 5 shows the light curves of J2150−0551 from the four deep X-ray observations X1, C1, X2, and C2. We obtained χ^2 probabilities of constancy of 0.07, 1.0, 0.02, and 0.48 for these light curves, respectively, indicating no significant short-term variability in all observations.

Multi-wavelength Photometry Observations

The photometry of J2150−0551 in various filters is listed in Supplementary Table 2 and plotted in Supplementary Figure 6. The source appeared red in the CFHT/CFH12K images in 2000–2001 but became blue in the CFHT/MegaCam images in 2005. It seemed to become red again in our new SOAR, Subaru, and Gemini images in 2014–2016. The change was thus more significant at shorter wavelengths, by $\sim$0.8 mag in the g' band and $\sim$0.3 mag in the r' band. The *HST*/ACS F775W photometry in September 2003 was consistent with the CFHT/CFH12K photometry, but not with the CFHT/MegaCam photometry. Therefore, the optical variability indicates that the outburst activity of J2150−0551 began before June 2005 (i.e., about one year before X1 or earlier) but after September 2003.

The CFHT/CFH12K photometry would then represent the quiescent emission of the optical counterpart to J2150−0551. The absolute V-band magnitude of the source would be ~ -12.3 AB mag if it is in Gal1. Therefore J2150−0551 most likely resides in a massive star cluster. In order to assess the properties of the cluster, we fitted the CFHT/CFH12K and *HST*/ACS photometry with a stellar population model[11] that is based on theoretical atmospheres with the Salpeter initial mass function. We applied both Galactic dust reddening of $\rm E(B-V)_G = 0.03$ mag and the intrinsic reddening of $\rm E(B-V)_i = 0.01$ mag. The intrinsic reddening was calculated based on the relation $\rm E(B-V) = 1.7 \times 10^{-22} N_H$ and using intrinsic $N_{\rm H}$ obtained from the X-ray spectral fits. The redshift of $z = 0.055$ was applied. We inferred a stellar population of age 1.0 ± 0.3 Gyr and bolometric luminosity $L_* = 1.4 \times 10^7\ L_\odot$, assuming a solar metallic-

ity. Using the mass-to-light ratio for the corresponding metallicity and age[1], we estimated the stellar mass of the cluster to be $M_* = 8.0 \times 10^6$ $M_\odot$. We also tested a two-population solution with the age of one population fixed at 14 Gyr. We found that we could not constrain the individual populations well and could not rule out a cluster composed of a dominant old population ($M_* \sim 5 \times 10^7$ $M_\odot$) and a small young population ($M_* \sim 4 \times 10^5$ $M_\odot$). Finally, we checked the fit with a metal poor population of metallicity [Z/H]=-1.35 and inferred a population of age 10^{+5}_{-4} Gyr, $M_* \sim 2.9 \times 10^7$ $M_\odot$, and $L_* \sim 1.3 \times 10^7$ $L_\odot$. The various fits suggest the cluster to have $M_* \sim (0.8\text{–}5.0) \times 10^7$ $M_\odot$ and $L_* \sim 1.4 \times 10^7$ $L_\odot$. The inferred population age has large uncertainties, strongly dependent on the population model assumed.

The enhancement of the flux at short optical wavelengths in 2005 could be from an irradiated accretion disk near the peak of the outburst, while radiation-driven outflow/wind could also cause this. In order to check roughly whether the optical flare could be described with disk irradiation, we fitted the broad-band spectra combining the X1 X-ray spectrum and the CFHT/MegaCam and CFHT/WIRCam photometry with the irradiated accretion disk model *diskir*[77] (in XSPEC), with an additional component to account for the star cluster emission. The star cluster component was fixed at the single stellar population model based on the CFHT/CFH12K and *HST*/ACS photometry, obtained above with a solar metallicity. The irradiated accretion disk model included thermal emission from the inner disk and reprocessing in the outer disk, but not the Compton tail, as the X-ray spectrum seemed purely thermal. The best-fitting model is shown in Supplementary Figure 6. The fraction of the bolometric flux that was thermalized in the outer disk was inferred to be $f_{\rm out} = 1.4^{+1.6}_{-0.4} \times 10^{-3}$, which is close to the typical values of $\sim 10^{-3}$ seen in BH X-ray binaries[77]. The best-fitting outer disk radius $r_{\rm out}$ was $10^{3.9\pm0.3}$ times the inner disk radius. We note that the CFHT/MegaCam photometry was taken before X1 and could correspond to a higher X-ray flux and that there could be hot outflow which we neglected in the modeling. Then we expect the real disk to assume smaller values of $r_{\rm out}$ and/or $f_{\rm out}$ than obtained above.

The model obtained from the broad-band fit above predicted the flux in the OM $UVM2$ filter to be one order of magnitude lower than the 3σ detection limit of the OM $UVM2$ images in X1 and X2 ($\sim$22.0 AB mag), explaining the non-detection of our source in these images. The 3σ detection limit (24.2 AB mag) of the $UVW2$ image in S1 is a factor of $\sim$2 above the prediction from the broad-band fit. Further considering the significant decrease of the source X-ray flux from X1 to S1, we expect the $UVW2$ flux in S1 to be much lower than the detection limit, explaining the non-detection of our source in the S1 $UVW2$ image.

The GMOS Observation

Supplementary Figure 7 plots the Gemini spectrum of the nuclear region of Gal1. The spectrum showed prominent absorption features, and thus we expect it to be dominated by an old stellar population. This is supported by the pPXF fit, which inferred the mean age weighted by the mass to be 10.9 Gyr and the mean age weighted by the light to be 10.4 Gyr (Supplementary Figure 8). Some faint emission lines were detected too, most significantly [N II] λ6583 (luminosity $L = 9 \pm 1 \times 10^{39}$ erg s^{-1}, 1σ error; [N II] λ6547 was affected by the atmospheric OH absorption) and the [S II] doublet (total $L = 9 \pm 1 \times 10^{39}$ erg s^{-1}). Hα were weaker, with $L = 5 \pm 1 \times 10^{39}$ erg s^{-1}. The emission lines in the Hβ-[O III] region, if present, were very weak (both [O III] λ4969 and λ5007 had $L = 3 \pm 1 \times 10^{39}$ erg s^{-1} and Hβ had $L < 3 \times 10^{39}$ erg s^{-1}, 3σ upper limit). The emission lines are probably due to nuclear activity, because [N II] λ6583 was stronger than Hα and we also detected a nuclear hard X-ray source (Source 1). The pPXF fit inferred the total stellar mass of Gal1 to be 2.3×10^{11} $M_\odot$ and the total stellar light within the fitting band (rest-frame 4400–7000 Å) to be 1.5×10^{10} $L_\odot$, which has been corrected for the slit loss by comparing the spectrum with the SDSS r'-band photometry.

The spectrum of Gal2 is shown in Supplementary Figure 9, and it is somewhat noisy. There were no significant emission lines or absorption features that would allow us to determine the redshift of the galaxies. In the pPXF fit shown in figure, we assumed Gal2 to have the same redshift as Gal1. The spectrum appeared blue, and our pPXF fit suggests the presence of young stellar populations ($\lesssim$ 0.3 Gyr, Supplementary Figure 10). The mean age of Gal2 weighted by the mass is 7.6 Gyr, while the mean age weighted by the light is 2.5 Gyr. The total mass is 1.1×10^8 $M_\odot$, and the luminosity within the fitting band is 4.7×10^7 $L_\odot$.

The spectrum of the optical counterpart to J2150$-$0551 is even noisier. There were no clear emission lines or absorption features in this spectrum either. In the pPXF fit shown in Supplementary Figure 11, we assumed J2150$-$0551 to be blueshifted by 300 km s^{-1} relative to Gal1 so that the Hα line corresponded to a spike in the spectrum. In this case, there might be some Hα emission at $L = 2.1 \pm 0.4 \times 10^{38}$ erg s^{-1}. The absence of strong narrow emission lines in J2150$-$0551 could be due to the lack of a narrow-line region as seen in AGNs and/or due to very weak persistent emission. The 3σ upper limit for [O III] λ5007 was 2×10^{37} erg s^{-1}. Based on the relation[78] between the bolometric persistent luminosity and the [O III] λ5007 luminosity for AGNs, we inferred the bolometric persistent luminosity in J2150$-$0551 to be $<1.7 \times 10^{39}$ erg s^{-1} (3σ upper limit), which is a factor of $\sim$6,000 below the peak luminosity of J2150$-$0551.

Because the spectrum is too noisy, the mass and light distributions inferred from the pPXF fit probably have large uncertainties. Thus we do not show them here. The pPXF fit inferred the optical counterpart to J2150$-$0551 to have a total stellar mass of 4.9×10^7 $M_\odot$, and stellar light within the fitting band of 5.7×10^6 $L_\odot$. The mean age weighted by the mass is 7.8 Gyr, and the mean age weighted by the light is 5.8 Gyr. These values are broadly consistent with those obtained from the fit to the CFHT/CFH12K and *HST* 2000–2003 photometry with a single stellar population model. In Supplementary Figure 11, we also mark the positions of the typical emission/absorption features expected if the source is a Galactic object of zero redshift. We could not confidently identify any feature in this case either.

The off-center IMBH Explanation

We have fitted the X-ray spectra of J2150$-$0551 assuming it to be in Gal1. All the results are well explained if it is a TDE from an IMBH of mass $\sim 5 \times 10^4$ $M_\odot$. The IMBH nature is strongly supported because the X-ray spectra can be described with a standard thermal thin disk of very high luminosities and low temperatures, which approximately follow the $L \propto T^4$ relation. Such a relation, though commonly observed in accreting stellar-mass BH in the thermal state[8,9], was not clearly observed in other IMBH candidates except[29,30] ESO 243-49 HLX-1. The position of the $L \propto T^4$ relation in the L–T plot and thus the disk temperature range (0.14–0.28 keV in J2150$-$0551) depend mainly on the BH mass. Therefore the similar $L \propto T^4$ relations traced out by ESO 243-49 HLX-1 and J2150$-$0551 (Figure 3) suggest that they contain BHs of similar masses, within a factor of a few.

The IMBH nature of J2150$-$0551 can also be inferred based on comparison of its disk temperatures with those seen in TDEs from galactic nuclei. Nuclear TDEs with good thermal X-ray spectra have peak disk temperatures in the range[6,79–82] between 0.05–0.15 keV (for studies that used a single-temperature blackbody to fit the X-ray spectra, we have multiplied the blackbody temperature by a factor of 1.4 to infer the equivalent disk temperature[83]). The peak disk temperature of J2150$-$0551 (0.28 keV) was at least twice higher than this range.

[1] http:www.maraston.eu

Because the disk temperature depends on the BH mass as $M^{-1/4}$ for a standard thermal thin disk[84], the mass of the BH in J2150−0551 would then be at least one order of magnitude lower than seen in most nuclear TDEs and thus is most likely in the IMBH range.

We note that J2150−0551 is unlikely to be one of ultraluminous X-ray pulsars, whose luminosities have been detected[85] to be up to 10^{41} erg s^{-1}. The ultrasoft X-ray spectra (photon index $\geq$4.8) of J2150−0551 are in contrast with the very hard spectra (photo index $<$2.0 below 5 keV) of four known ultraluminous X-ray pulsars[85,86].

Our multiwavelength data suggest that J2150−0551 exhibited a luminous prolonged outburst from optical to soft X-rays. The outburst was probably not caused by large variability of persistent emission, which might be very weak based on the lack of strong narrow emission lines (see the previous section). The high luminosity and the long duration of the outburst can be naturally explained if the event is a TDE. A simple TDE model for the luminosity evolution of J2150−0551 is plotted in Figure 2. It models the decay as $(t-t_{\rm D})^{-5/3}$, which was predicted by the standard TDE theory[1,15] and observed in many TDE candidates in galactic nuclei[87,88]. The disruption time $t_{\rm D}$ was inferred to be around 18 October 2003 (1σ error 37 days). The very small number of data points that we had did not allow us to fit the light curve with more complicated models. If we fitted the luminosity decay as $(t-t_{\rm D})^{\alpha}$ with a variable index α, we obtained a fit of $\alpha=-0.8\pm0.1$ (1σ error), but via the F-test, a variable index only improved the fit at the 74% confidence level. Moreover, the disruption time was inferred to be on 24 August 2005 (1σ error 47 days), within the time interval when the optical flare was detected. Similarly, with so few data points, it is difficult to check for the presence of slow circularization. When circularization of stellar debris is slow, the light curve would decline slower than predicted in the standard TDE theory[17], as might occur in the TDE candidate[6] 3XMM J150052.0+015452. Given that the luminosity evolution of J2150−0551 is consistent with the standard $(t-t_{\rm D})^{-5/3}$ curve, we expect relatively prompt circularization of stellar debris in this event.

There could be a super-Eddington accretion phase in J2150−0551 lasting for around three years. This is supported by the X1 observation, which seems to deviate from the $L\propto T^4$ relation traced out by the other observations. The luminosity in the super-Eddington accretion phase is expected to be around the Eddington limit[16]. This can explain the non-detection of the source in the *XMM-Newton* slew observation in 2004 (Figure 2). In the optical flare phase detected in 2005, the u^*-band flux in June 2005 was close to that expected from the g' and r' fluxes in November 2005, which also supports a constant luminosity in the super-Eddington accretion phase, while the mass accretion rate was expected to decrease by 50% in this period (Figure 2). The super-Eddington accretion phase can last[89] $t_{\rm Edd}\approx 1.9(\eta/0.1)^{3/5}M_6^{-2/5}m_*^{1/5}x_*^{3/5}$ yr, where $M_6=M_{\rm BH}/10^6\ M_\odot$, η is the radiative efficiency, m_* is the mass of the star in units of $M_\odot$, and x_* is the radius of the star in units of $R_\odot$. Assuming typical parameters of $\eta=0.1$, $m_*=1.0$, and $x_*=1.0$, we have $t_{\rm Edd}=12.0$ yr and 4.8 yr for $M_{\rm BH}=10^4\ M_\odot$ and $10^5\ M_\odot$, respectively. Therefore our inference of $t_{\rm Edd}\sim3$ yr for J2150−0551 is reasonable for its IMBH nature. Because of the presence of a long super-Eddington accretion phase, which was largely missed, J2150−0551 appeared to last longer than other TDEs (typically decay significantly in a year).

The optical counterpart in quiescence is consistent with a massive ($\sim10^7\ M_\odot$) star cluster with an effective radius of $<$20 pc. This dense star cluster environment makes the TDE explanation for J2150−0551 reasonable. One intriguing explanation for the optical counterpart is that it is the accreted remnant nucleus of a dwarf galaxy tidally stripped by Gal1. Accreted remnant nuclei of dwarf galaxies have been used to explain massive star clusters brighter than classical globular clusters[90–93]. Interestingly, Figure 1 shows a possible minor merger of a satellite galaxy (Gal2), which is connected with Gal1 through a possible stream and is close to J2150−0551. The nuclei are normally expected to remain in the middle of the tidal stream in minor mergers[94]. Thus Gal2 is probably unrelated to J2150−0551. However, the presence of such a merging feature indicates that Gal1 might be in an epoch of frequent minor mergers.

A few optical transients possibly offset from the centers of their host galaxies were reported as TDE candidates (PTF-10iam, PTF-10nuj, PTF-11glr, and Dougie)[95,96], but it is very hard to completely rule out a supernova explanation for them[97], due to the lack of strong X-ray detections associated with these events[98]. The event 3XMM J141711.1+522541 could be an off-center TDE with a peak X-ray luminosity of a few $\sim10^{43}$ erg s^{-1}, but the TDE nature of that event was not certain due to poor sampling of the light curve[36]. Therefore, J2150−0551 is the best off-center TDE candidate thus far.

A wide variety of searching strategies[99–101] have resulted in discovery of a few off-center[27–30,36,102–107] and centered[108–112] IMBH candidates. These objects were generally not bright in X-rays, except ESO 243-49 HLX-1 and some others that could be due to TDEs[24,36,110,113]. ESO 243-49 HLX-1 and J2150−0551 showed the best evidence for the thermal state of an IMBH, with a clear $L\propto T^4$ evolution track detected.

Alternative Explanations

At a high Galactic latitude of -42°, J2150−0551 has a high chance to be extragalactic. We have explored the case that the source is in Gal1. We still need to check whether the source could be instead from the nucleus of a background galaxy, either as an AGN or TDE, that just happens to lie very close to Gal1 in the sky. J2150−0551 is different from standard AGNs in various aspects, with very soft X-ray spectra ($\Gamma_{\rm PL}>4.5$), large variability (a factor of $\sim$17, absorbed 0.2–12 flux), and a large X-ray (0.2–12 keV, maximum) to IR ($K_{\rm s}$-band) flux ratio ($\log(F_{\rm X}/F_{\rm IR})=3.2$), while most AGNs, including Narrow-line Seyfert 1 galaxies that might have accretion rates close to the Eddington limit, have[114] $\Gamma_{\rm PL}\sim1.9$, long-term variation factors <10, and $\log(F_{\rm X}/F_{\rm IR})\lesssim2.0$. Two AGN candidates (2XMM J123103.2+110648 and GSN 069) with AGN emission line signatures in optical were found to have pure thermal X-ray spectra and large variability, but the TDE explanation for them cannot be ruled out[109,114–118]. One main difference between J2150−0551 and these two and other thermal TDE candidates is that J2150−0551 had a significantly higher X-ray-to-IR flux ratio ($\log(F_{\rm X}/F_{\rm IR})=3.2$) than other thermal TDE candidates ($\log(F_{\rm X}/F_{\rm IR})\lesssim2.0$). Moreover, there are very few known thermal TDEs, especially those of high characteristic temperatures (peak temperature >0.2 keV). Then the chance probability to find one such TDE so close to Gal1 is very low ($\sim$0.01%). Based on the above argments, we rule out a background AGN or TDE explanation for J2150−0551.

If J2150−0551 is a Galactic object, given its high Galactic latitude, we expect the source distance to be small. Then it would most likely have low luminosities (0.2–12 keV luminosity $<5\times10^{32}$ erg s^{-1} assuming a distance of 2 kpc). J2150−0551 had $\log(F_{\rm X}/F_{\rm IR})=3.2$, making it unlikely to be a coronally active star ($\log(F_{\rm X}/F_{\rm IR})\lesssim-0.9$)[114]. High X-ray to IR flux ratios, however, are often seen in compact object systems that contain white dwarfs, NSs, or BHs[114]. With very soft X-ray spectra, the source cannot be a low-luminosity BH X-ray binary, whose X-ray spectra are expected to be hard ($\Gamma_{\rm PL}\lesssim2.0$)[119]. The large variability (a factor of 17 in $\sim$10 yr) of the source makes it unlikely to be an isolated white dwarf or NS. The low luminosities of the source would make it unlikely to be supersoft emission from cataclysmic variables ($\gtrsim10^{36}$ erg s^{-1})[120].

Then we are left with the cooling NS in a LMXB as the only likely alternative explanation for the source if it is in our Galaxy. As we

have shown above, the very soft X-ray spectra of J2150−0551 approximately resemble those of thermally cooling NSs in LMXBs often detected after large accretion outbursts[52]. Supplementary Figure 12 shows that the cooling curve of J2150−0551 (if it is an NS LMXB) is very similar to those of six confirmed LMXBs[51]. There are two major differences though. One is that J2150−0551 had a cooling timescale of 2008 days, much longer than the six NS LMXBs shown (<500 days). The other major difference is that the NS in J2150−0551 in the later stage would be much cooler (31 eV) than the NSs in those six LMXBs (>50 eV).

In the NS LMXB explanation for J2150−0551, the very faint optical flare detected in the CFHT images in 2005 would be probably associated with the accretion outburst, instead of the early fast-evolving thermal cooling phase. This is because the optical flux was steady during the flaring period (see the above section). Then we inferred the accretion outburst to last for at least five months and end at a time between 5 May 2006 (when X1 was taken) and 7 November 2005 (when the CFHT g'-band image was taken). The accretion outburst should have started after 14 May 2004 (when the first *XMM-Newton* slew observation was taken). This is because J2150−0551 was not detected in this slew observation, whose 3σ upper limit of the 0.2–12 keV flux was only a factor of four of the flux in X1. Our constraint on the accretion outburst start date is also supported by the absence of an optical enhancement in the *HST* observation in September 2003.

The quiescent optical/IR counterpart to J2150−0551 is very faint, with the $K_{\rm s}$-band Vega magnitude of at most 20.8 mag, or absolute magnitude between +8.1 and +9.1 mag assuming a source distance of 2.2–3.5 kpc (inferred from the *nsatmos* fits listed in Table 3). The companion counterpart is then expected to be a late M dwarf[121]. However, during quiescence, the optical spectrum of the source did not look very red, as would be expected for a late M dwarf. The most likely explanation for this would be that the companion was illuminated by the NS thermal emission.

Besides the very low chance probability of positional coincidence with Gal1, the most challenging problem with the cooling NS LMXB explanation for J2150−0551 is the absence of a large accretion outburst in the ASM light curve, which constrained the 3σ upper limit of the monthly-average 1.5–12 keV luminosity of J2150−0551 to be (3–9)$\times10^{34}$ erg s^{-1}, assuming a source distance of 2.2–3.5 kpc (Table 3). Then the accretion outburst would be very faint, making the source one of the very faint X-ray transients (VFXTs, peak X-ray luminosity $<10^{36}$ erg s^{-1}), most of which were detected toward the Galactic center[122–124]. Most VFXTs have very short outbursts of weeks, but quasi-persistent VFXTs also exist[125]. Cooling curves thus far were only detected for transient LMXBs that experience bright outbursts ($\gtrsim10^{36}$ erg s^{-1}). It is not clear whether the crust of an NS in a VFXT could be significantly heated up.

Our numerical modeling with `NSCool` of the hypothetical accretion outburst that may have resulted in the observed cooling curve of an NS in the LMXB J2150−0551 inferred the mass accretion rate $\dot{M}$ and thus ASM count rate $\dot{C}$ to strongly depend on the value of $Q_{\rm sh}$ assumed. The physical nature of the shallow heating is still unknown, and $Q_{\rm sh}$ inferred by fitting cooling curves of several LMXBs are mostly[58,62,126–128] <3 MeV/nucleon. The MCMC runs found $\dot{C} = 2.3^{+0.8}_{-0.5}$ cts s^{-1} (1σ error) for $Q_{\rm sh} = 1$ MeV and $\dot{C} = 0.8^{+0.3}_{-0.2}$ cts s^{-1} for $Q_{\rm sh} = 3$ MeV. These values are factors of 10 (11σ) and 4 (5σ) of the 3σ upper limit implied by the ASM ($\lesssim$0.2 cts s^{-1}), respectively. The discrepancy would be larger, further considering that our MCMC runs assumed a constant $\dot{M}$ in the accretion outburst, without taking into account the outburst decay, which would significantly underestimate[126] $Q_{\rm sh}$ and thus $\dot{M}$. If $Q_{\rm sh}$ was allowed to be extremely high (10 MeV/nucleon), it is possible to have a very faint accretion outburst ($\dot{C} = 0.21 \pm 0.04$ cts s^{-1}, around the ASM detection limit) to produce the observed cooling curve. However, thus far, only MAXI J0556−332, which is completely different from J2150−0551 for containing an extremely hot NS (the top dotted line in Supplementary Figure 12) and having super-Eddington accretion rates in the peak[51], was inferred to have[63,129] $Q_{\rm sh} \sim 10$ MeV/nucleon.

One way to differentiate between a Galactic cooling NS and a TDE by an extragalactic IMBH would be through continued multi-wavelength follow-up observations. NS LMXBs in quiescence might sporadically exhibit low-luminosity X-ray flares[51,130], which are not expected in a TDE. If it is a cooling NS, we expect the flux and the temperature to hardly decrease in the future, while for a TDE, we expect the flux to continue to decrease with time, approximately as $t^{-5/3}$.

IMBH Space Density

TDE rates can be used to probe the space density and the occupation fraction of BHs[131]. We roughly estimated the rate of off-center TDEs like J2150−0551, in a similar way as we did for another TDE candidate[6] 3XMM J150052.0+015452. We discovered J2150−0551 through systematic search over the 3XMM-DR5 catalog[132]. We were limited to the sources that have at least one detection of S/N > 20. We focused on sources of large variability and/or soft spectra and carefully inspected whether they are TDEs based on all available public data. Limited to observations outside the Galactic plane (galactic latitude $|b| > 20^\circ$) and assuming that events like J2150−0551 have a mean luminosity and soft X-ray spectra as in X1 and have a duration of 3 years, we estimated to detect $\sim2.0\times10^8 r$ events, where r is the event rate in units of Mpc^{-3} yr^{-1}. We at least discovered one event, suggesting $r \gtrsim 5\times10^{-9}$ Mpc^{-3} yr^{-1}. Our search was not complete in the sense that we could not confirm the off-center TDE nature of a few fainter events due to the poor X-ray coverage and/or the lack of deep optical data (needed to check the off-center nature of the events). For example, another event 3XMM J141711.1+522541 possibly similar to J2150−0551 was also discovered in this search[36]. Taking this into account, we estimated r to be around 10^{-8} Mpc^{-3} yr^{-1}.

The expected TDE rate γ of IMBHs of a few 10^4 $M_\odot$ in star clusters is not well established theoretically. Studies with direct N-body simulations[21,22] inferred $\gamma \sim 10^{-5}$ yr^{-1} per IMBH of a few 10^4 $M_\odot$, while analytical studies estimated[23,133,134] $\gamma \sim 10^{-3}$ yr^{-1}. Then based on the observed TDE rate above, we constrained the space density n of off-center IMBHs of a few 10^4 $M_\odot$ to be between $\sim10^{-5}$–10^{-3} Mpc^{-3}.

The space density n' of the off-center star clusters of mass $\geq10^7$ $M_\odot$, as observed in the counterpart to J2150−0551, can be estimated based on the dependence of the number of massive star clusters on the halo mass predicted from numerical simulations[135] and the halo mass function[136]. We estimated $n' \sim 10^{-2}$ Mpc^{-3}, which had been multiplied by a factor of 2 to account for the fact that the numerical simulations appeared to underestimate the number of massive star clusters in galaxy clusters by such a factor. Therefore, the space density of massive star clusters is, as expected, at least one order of magnitude larger than the space density of IMBHs of a few 10^4 $M_\odot$ estimated by us above based on the TDE rate.

Supplementary Table 1 | The X-ray Observation Log. Columns: (1) the observation ID with our designation given in parentheses, (2) the observation start date, (3) the instrument, (4) the off-axis angle, (5) the exposures of data used in final analysis, (6) the radius of the source extraction region, (7) the net count rate in the source extraction region (0.3–10 keV for *XMM-Newton* and *Swift* observations, and 0.4–8 keV for C1 and 0.3–8 keV for C2, all in the observer frame), with 90% confidence error.

Obs. ID (1)	Date (2)	Instrument (3)	OAA (arcmin) (4)	T (ks) (5)	$r_{\rm src}$ (arcsec) (6)	Count rate (10^{-3} counts s^{-1}) (7)
XMM-Newton:						
0404190101(X1)	2006-05-05	pn/MOS1/MOS2	7.1	24/50/50	35/25/25	$115.4 \pm 3.8/68.6 \pm 1.9/63.2 \pm 1.9$
0603590101(X2)	2009-06-07	pn/MOS1/MOS2	5.8	52/69/69	35/35/35	$97.8 \pm 2.5/22.6 \pm 1.0/22.5 \pm 1.0$
Chandra:						
6791(C1)	2006-09-28	ACIS-I0	8.1	101	7.7	49.0 ± 1.1
17862(C2)	2016-09-14	ACIS-S3	0.15	77	1.6	2.0 ± 0.3
Swift:						
00033396001–2(S1)	2014-09-05	XRT	2.4	8.0	20	$0.74^{+0.67}_{-0.45}$

Supplementary Table 2 | The Optical/IR Observation Log and Photometry. Columns: (1) the telescope, (2) the observation start date, (3) the instrument, (4) the filter, (5) effective wavelength, (6) full width at the half maximum; (7) the exposure time; (8) the AB magnitude with 1σ error. [a]The exposure time is half of that of the observation, because our source was in the CCD gap half of the time. [b]Including two exposures (each of 840 s) in August–September 2001. [c]Including two exposures (each of 510 s) in August–September 2001.

Telescope	Date	Instrument	Filter	$\lambda_{\rm eff}$ (Å)	$\Delta\lambda_{\rm FWHM}$ (Å)	T (s)	Magnitude (AB mag)
(1)	(2)	(3)	(4)	(5)	(6)	(7)	(8)
HST	2003-09-13	ACS	F775W	7653	1517	1020[a]	23.87 ± 0.03
CFHT	2000-08-03	CFH12K MOSAIC	B	4302	990	7080[b]	25.27 ± 0.08
	2000-08-01	CFH12K MOSAIC	V	5338	974	7440	24.60 ± 0.06
	2000-08-03	CFH12K MOSAIC	R	6516	1250	7080[c]	24.07 ± 0.04
	2000-08-01	CFH12K MOSAIC	I	8090	2164	21600	23.78 ± 0.03
	2005-06-03	MegaCam	u^*	3882	654	7040	24.41 ± 0.05
	2005-11-07	MegaCam	g'	4767	1434	744	24.03 ± 0.10
	2005-11-07	MegaCam	r'	6192	1219	480	23.70 ± 0.07
	2005-11-07	MegaCam	z'	8824	934	360	23.43 ± 0.16
	2009-06-14	WIRCam	$K_{\rm s}$	21338	3270	900	22.64 ± 0.10
SOAR	2014-11-26	Goodman Spectrograph	U	3664	653	2400	25.97 ± 0.39
Subaru	2014-12-19	Suprime-Cam	g'	4619	1390	535	24.78 ± 0.07
Gemini	2016-08-06	Gemini-S	$r_{\rm G0326}$	6244	1415	720	24.04 ± 0.04

Supplementary Table 3 | Fitting results of the X-ray spectra from J2150−0551. All errors are at the 90% confidence level. $N_{\rm diskpbb}$ is defined as $((R_{\rm in}/{\rm km})/(D/10{\rm kpc}))^2 \cos\theta$, where $R_{\rm in}$ is the apparent inner disk radius, D is the source distance, θ is the disk inclination. [a]These parameters were tied together in the simultaneous fits to the X1, C1, and X2 spectra, and they were fixed at the best-fitting values when we calculated uncertainties of other spectral parameters.

	X1	C1	X2	C2
Model: diskpbb				
$N_{\rm H,i}$ (10^{20} cm^{-2})[a]		1.2 ± 0.8		...
$kT_{\rm diskpbb}$ (keV)	$0.283^{+0.003}_{-0.003}$	$0.281^{+0.004}_{-0.004}$	$0.230^{+0.002}_{-0.002}$	...
$p_{\rm diskpbb}$	$0.61 \pm 0.01^{+0.012}_{-0.012}$	0.71 ± 0.03	0.75(fixed)	...
$N_{\rm diskpbb}$[a]		7.5 ± 1.2		...
$\chi^2_\nu(\nu)$	0.99(326)	1.28(101)	0.96(361)	...
Model: optxagnf ($a^* = 0.92$, pure thermal disk)				
$N_{\rm H,i}$ (10^{20} cm^{-2})[a]	...	$0.4^{+0.5}$		...
$M_{\rm BH}$ ($M_\odot$)	...	$5.3 \pm 0.4 \times 10^4$		...
$L_{\rm bol}/L_{\rm Edd}$	...	1.003 ± 0.034	0.409 ± 0.015	...
$\chi^2_\nu(\nu)$	...	1.29(100)	0.96(360)	...
Model: optxagnf (maximally-rotating, pure thermal disk)				
$N_{\rm H,i}$ (10^{20} cm^{-2})[a]	...	1.5 ± 1.0		...
$M_{\rm BH}$ ($M_\odot$)	...	$1.2 \pm 0.1 \times 10^5$		...
$L_{\rm bol}/L_{\rm Edd}$	...	0.406 ± 0.014	0.167 ± 0.006	...
$\chi^2_\nu(\nu)$	...	1.29(100)	0.96(360)	...
Model: nsatmos ($M_{\rm NS} = 1.4\ M_\odot$, $R_{\rm NS} = 10$ km)				
$N_{\rm H,i}$ (10^{20} cm^{-2})[a]		3.3 ± 0.8		
$kT_{\rm eff}^\infty$ (eV)	74.6 ± 0.5	70.0 ± 0.3	55.7 ± 0.5	37.5 ± 0.9
$D_{\rm nsatmos}$ (kpc)[a]		2.2 ± 0.2		
$\chi^2_\nu(\nu)$	1.10(327)	1.34(102)	1.02(361)	3.18(8)
$L_{\rm bol}$ (10^{32} erg s^{-1})	6.78 ± 0.18	5.26 ± 0.10	2.11 ± 0.08	0.43 ± 0.04
Model: nsatmos ($M_{\rm NS} = 1.4\ M_\odot$, $R_{\rm NS} = 13$ km)				
$N_{\rm H,i}$ (10^{20} cm^{-2})[a]		3.1 ± 0.8		
$kT_{\rm eff}^\infty$ (eV)	76.3 ± 0.5	71.5 ± 0.4	57.0 ± 0.5	38.3 ± 0.9
$D_{\rm nsatmos}$ (kpc)[a]		2.7 ± 0.2		
$\chi^2_\nu(\nu)$	1.11(327)	1.34(102)	1.03(361)	3.14(8)
$L_{\rm bol}$ (10^{32} erg s^{-1})	10.80 ± 0.29	8.36 ± 0.17	3.36 ± 0.12	0.69 ± 0.06
Model: nsatmos ($M_{\rm NS} = 1.4\ M_\odot$, $R_{\rm NS} = 16$ km)				
$N_{\rm H,i}$ (10^{20} cm^{-2})[a]		2.8 ± 0.8		
$kT_{\rm eff}^\infty$ (eV)	78.5 ± 0.5	73.6 ± 0.4	58.6 ± 0.5	39.3 ± 0.9
$D_{\rm nsatmos}$ (kpc)[a]		3.5 ± 0.3		
$\chi^2_\nu(\nu)$	1.11(327)	1.34(102)	1.03(361)	3.13(8)
$L_{\rm bol}$ (10^{32} erg s^{-1})	16.90 ± 0.45	13.08 ± 0.25	5.22 ± 0.19	1.06 ± 0.10

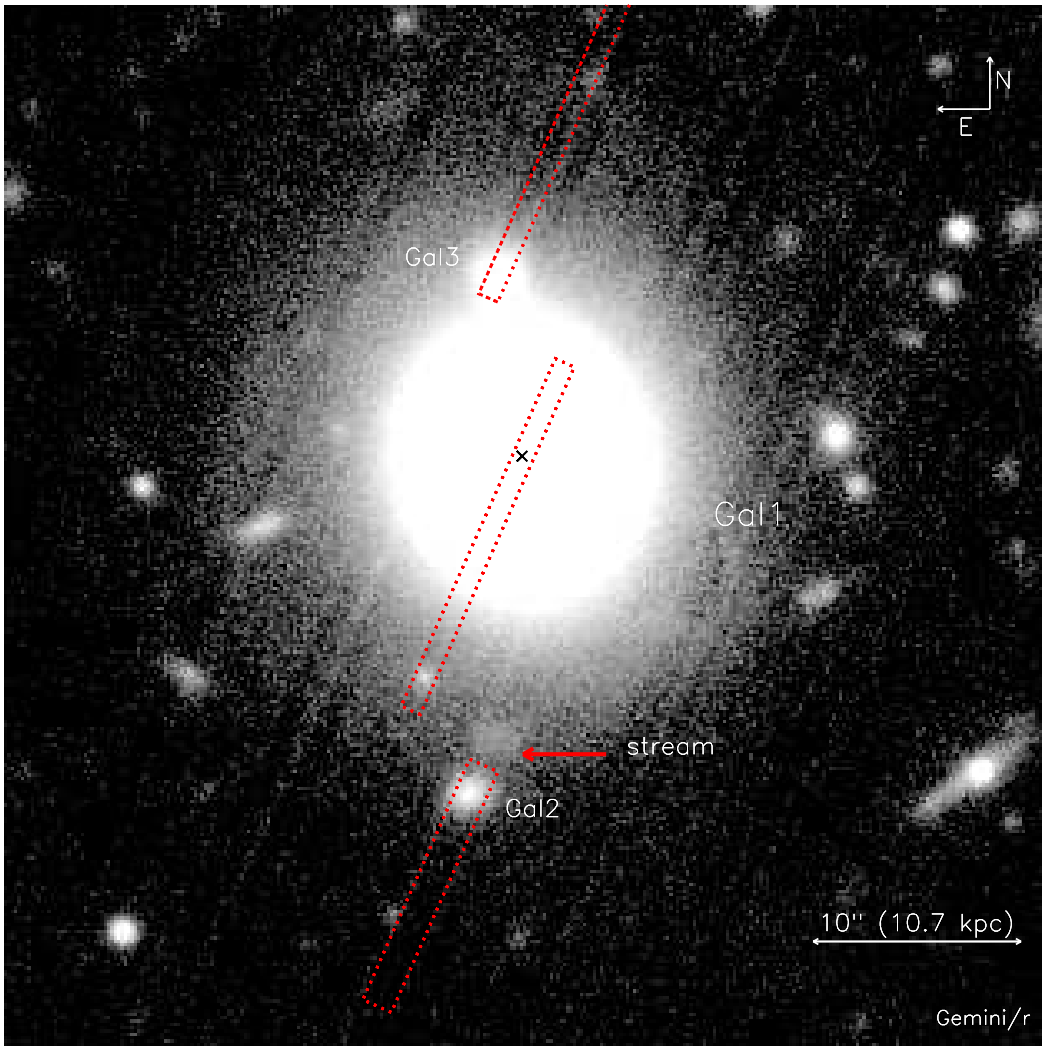

Supplementary Figure 1 | The Gemini image used to make the slits for a GMOS observation around the field of J2150−0551. Three slits are shown here, with one going through the nucleus of Gal1 and the counterpart to J2150−0551, one for Gal2, and one for a possible background galaxy Gal3 (marked in the plot, not studied in this work).

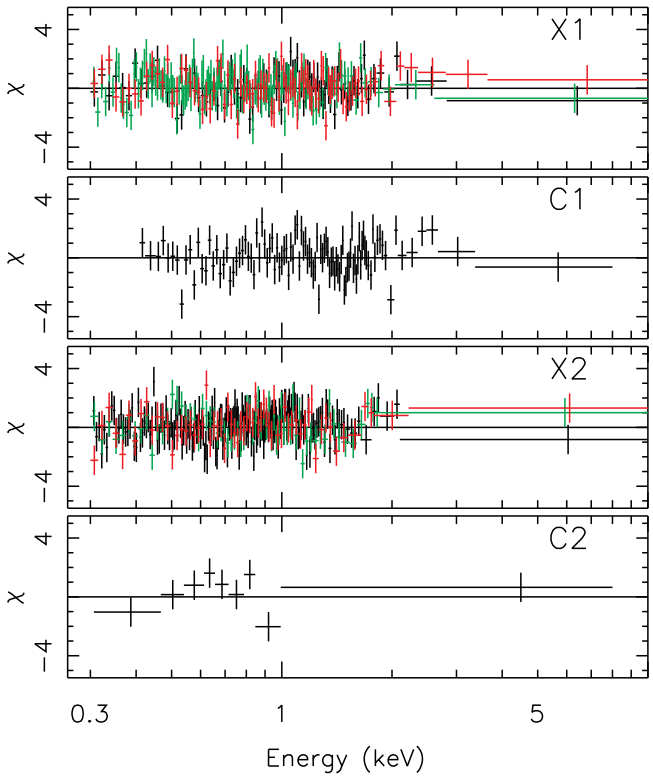

Supplementary Figure 2 | The residuals of the absorbed *diskbb* fits shown in Figure 2, in units of standard deviations with error bars of size one. The pn, MOS1, and MOS2 data in X1 and X2 are shown in black, red, and green, respectively.

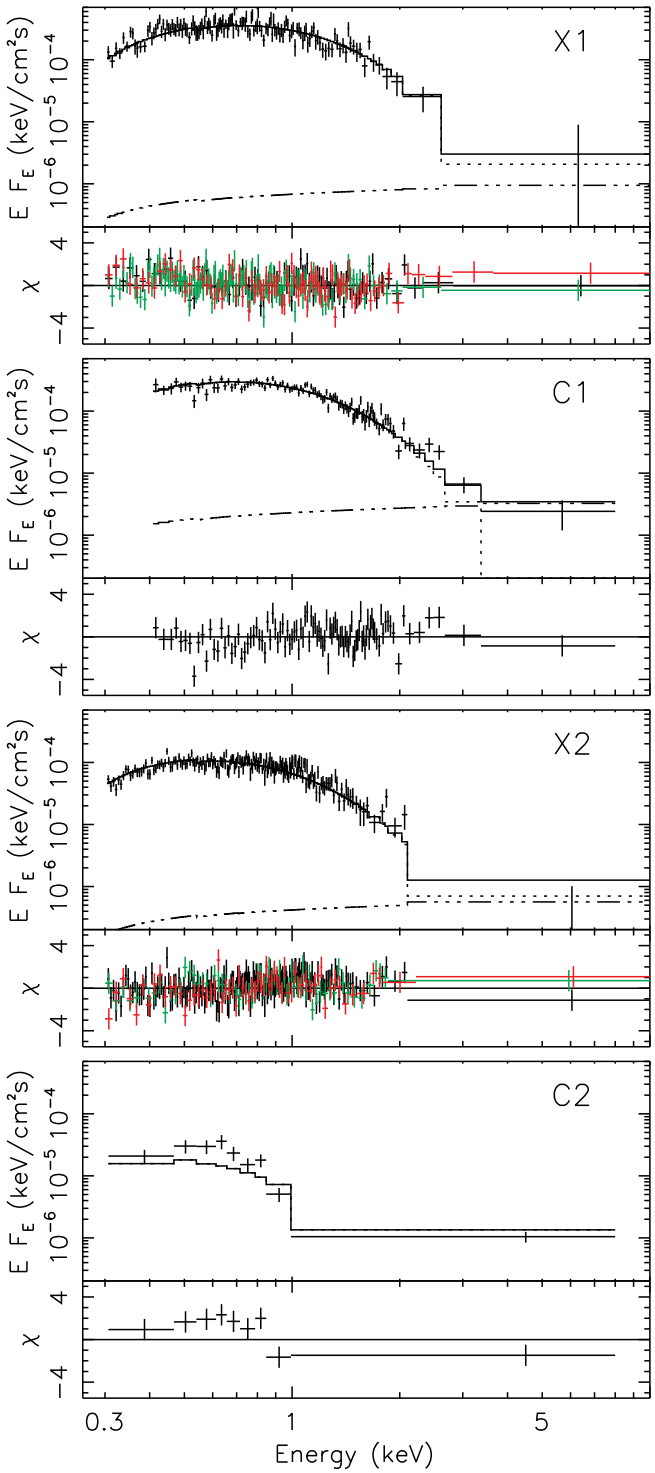

Supplementary Figure 3 | The unfolded spectra (black data points with 1σ error bars) and fit residuals (in units of standard deviations with error bars of size one) of *XMM-Newton* and *Chandra* observations, similar to the *diskbb* fits shown in Figure 2 and Supplementary Figure 2 but for an absorbed *nsatmos* model. Note that the fits to the X1, C1, and X2 spectra also include a PL of $\Gamma_{\rm PL} = 1.8$ to account for possible contamination from the faint nuclear source of Gal1 (Source 1). All error bars represent 1σ uncertainties.

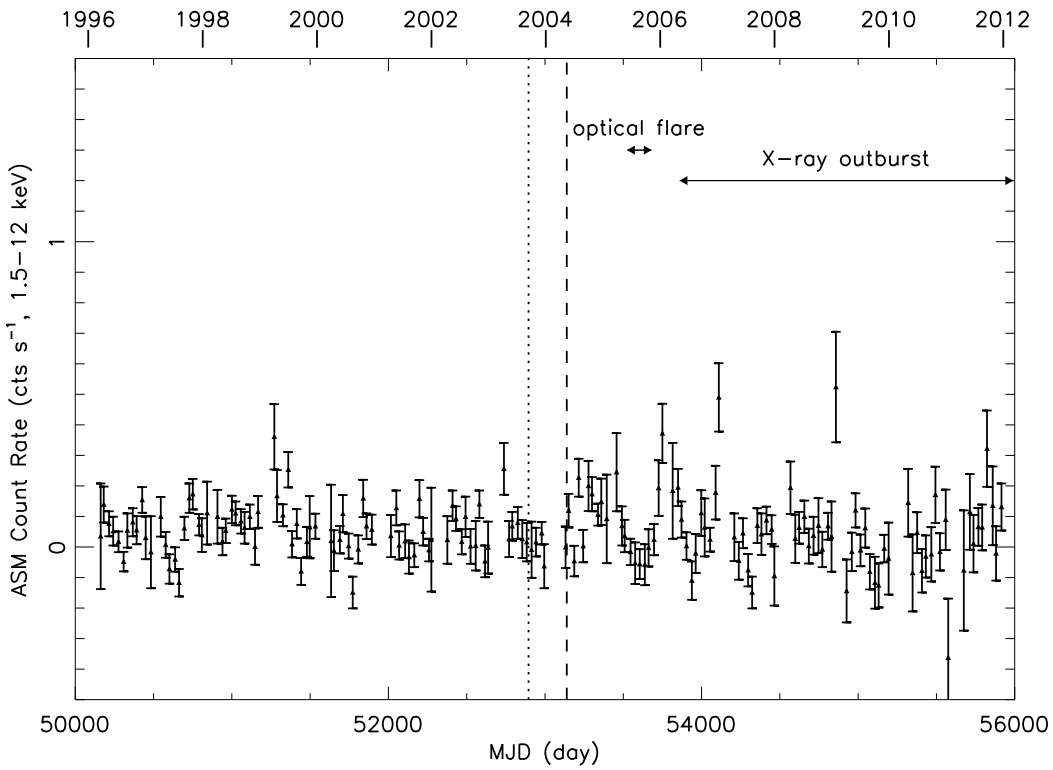

Supplementary Figure 4 | The ASM monthly light curve of J2150−0551, indicating no significant emission at any time of the mission. Error bars represent 1σ uncertainties. The dotted vertical line marks the time of the *HST*/ACS F775W observation (the optical flare should have started later than this), and the dashed vertical line marks the time of the *XMM-Newton* slew observation on 14 May 2004 (the accretion outburst of J2150−0551, if it is an NS LMXB, should have started later than this). Time ranges of the optical flare detected by the CFHT and the X-ray outburst detected by *XMM-Newton* and *Chandra* are also marked. The X-ray outburst was not detected by the ASM because its peak flux was three orders of magnitude below the ASM sensitivity limit.

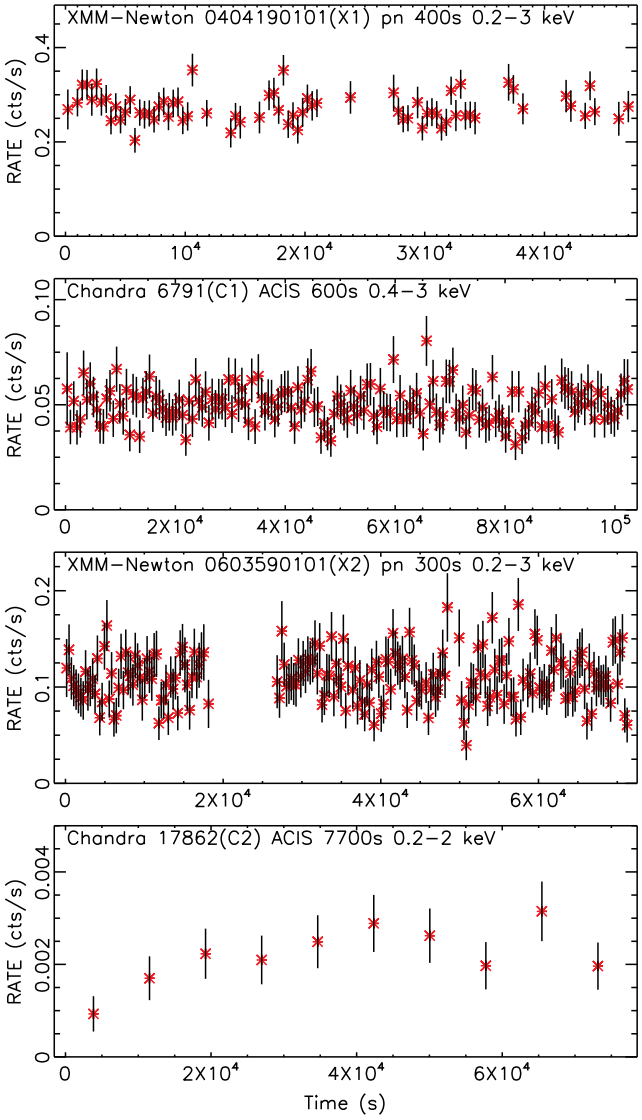

Supplementary Figure 5 | The background subtracted light curves of J2150−0551 from X1, C1, X2, and C2. Error bars represent 1σ uncertainties. The instrument, light curve bin size, and energy band used for each light curve are noted in the plot. The source showed no significant short-term variability in any observation.

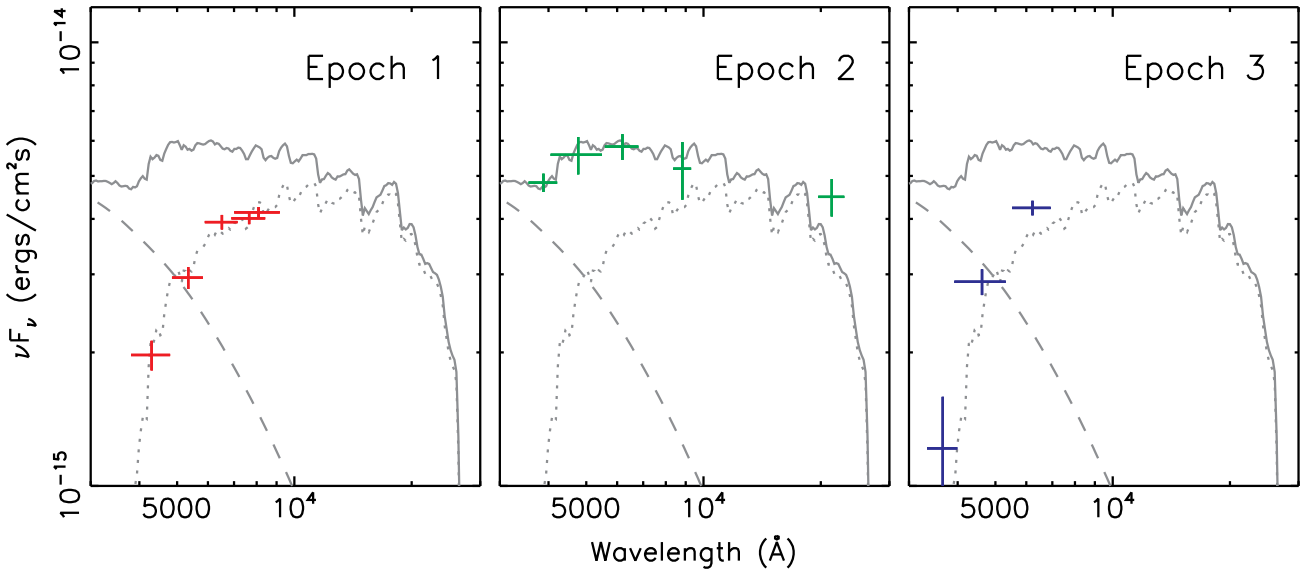

Supplementary Figure 6 | The optical/IR photometry (and 1σ error bars) of J2150−0551 in various epochs, indicating the presence of an optical flare in 2005. Left panel: the CFHT/CFH12K (2000–2001) and *HST*/ACS F775W (2003) photometry. Middle panel: the CFHT/MegaCam optical (2005) and WIRCam Ks (2009) photometry (green data). Right panel: the SOAR, Subaru, and Gemini photometry in 2014–2016. The gray solid line in all panels shows the fit to the broad-band spectrum combining X1, the CFHT/MegaCam and WIRCam photometry, with an irradiated disk (gray dashed line) plus a stellar population emission component (gray dotted line, inferred from the CFHT/CFH12K and *HST*/ACS photometry in 2000–2003).

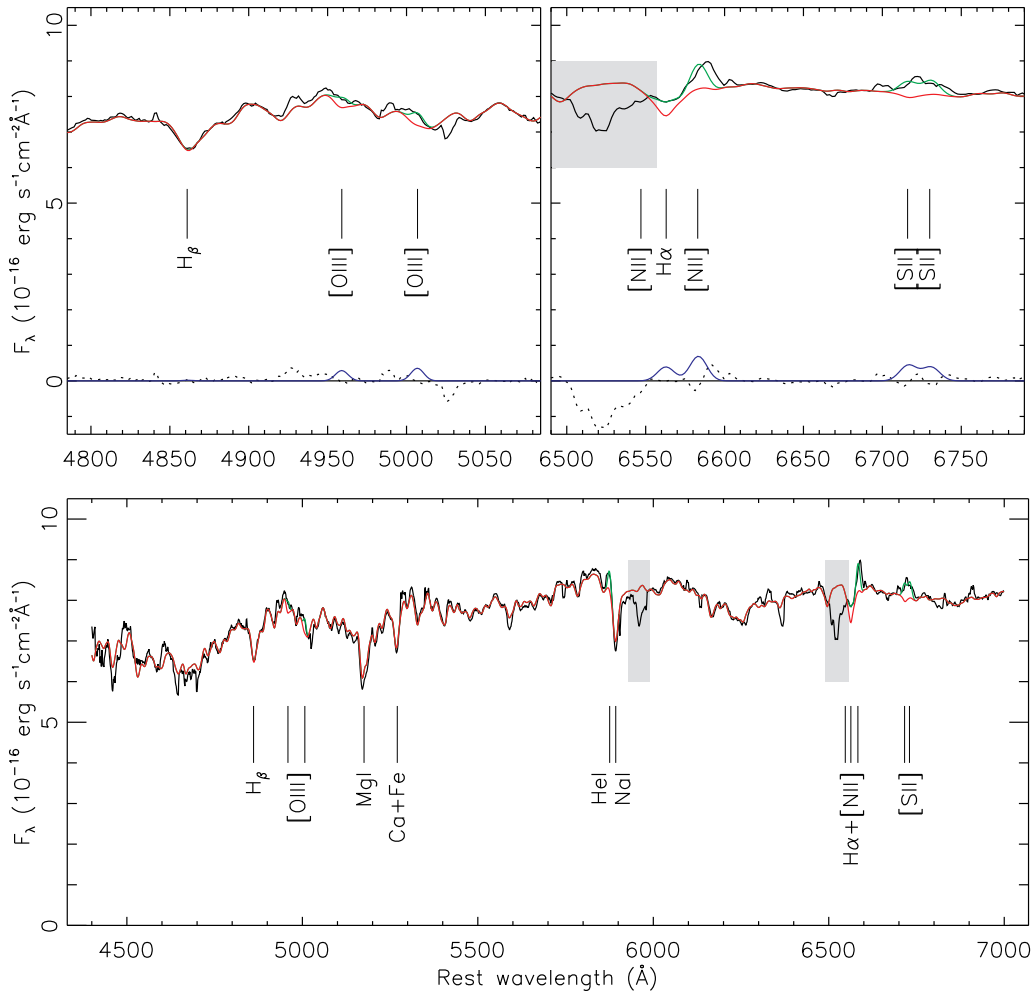

Supplementary Figure 7 | The pPXF fit to the Gemini spectrum around the nuclear region of Gal1, with the pPXF fit shown as a solid green line and the star component shown as a red line. The upper two panels zoom into the Hβ-[O III] complex and the Hα-[N II] region, including the fit residuals (dotted lines) and the Gaussian gas lines (blue solid lines). The gray areas mark the regions where the spectrum was seriously affected by the atmospheric OH absorption and CCD gap.

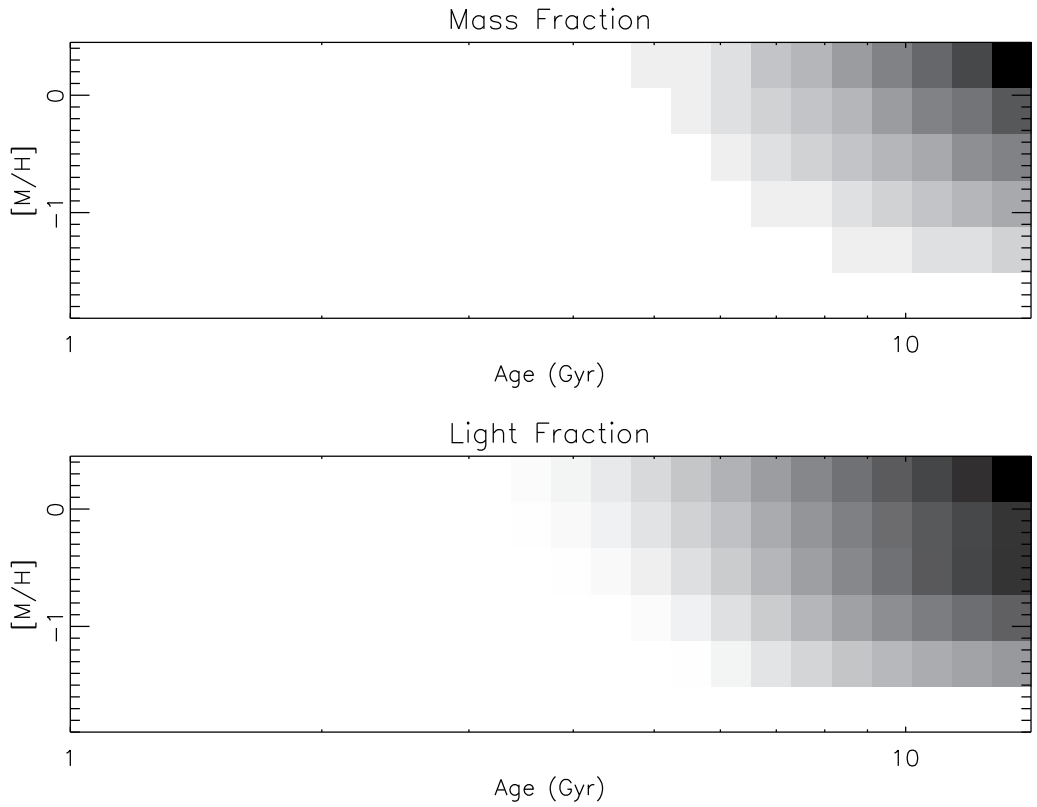

Supplementary Figure 8 | Relative mass and light fractions of stellar populations in the nuclear region of Gal1 with respect to metallicity and age. Darker shading indicates a larger mass fraction in the best-fitting model. The light was integrated over 4400–7000 Å.

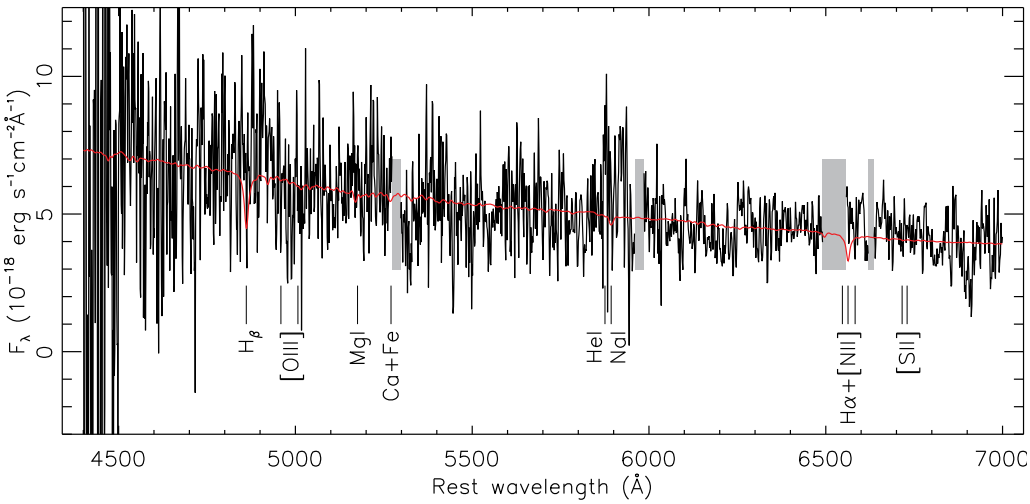

Supplementary Figure 9 | The pPXF fit to the Gemini spectrum of Gal2, assuming it to be at the same redshift as Gal1. The spectrum is somewhat noisy, and we observed no significant emission lines or absorption features. The gray areas mark some portions of the spectra seriously affected by the atmospheric OH absorption and CCD gaps.

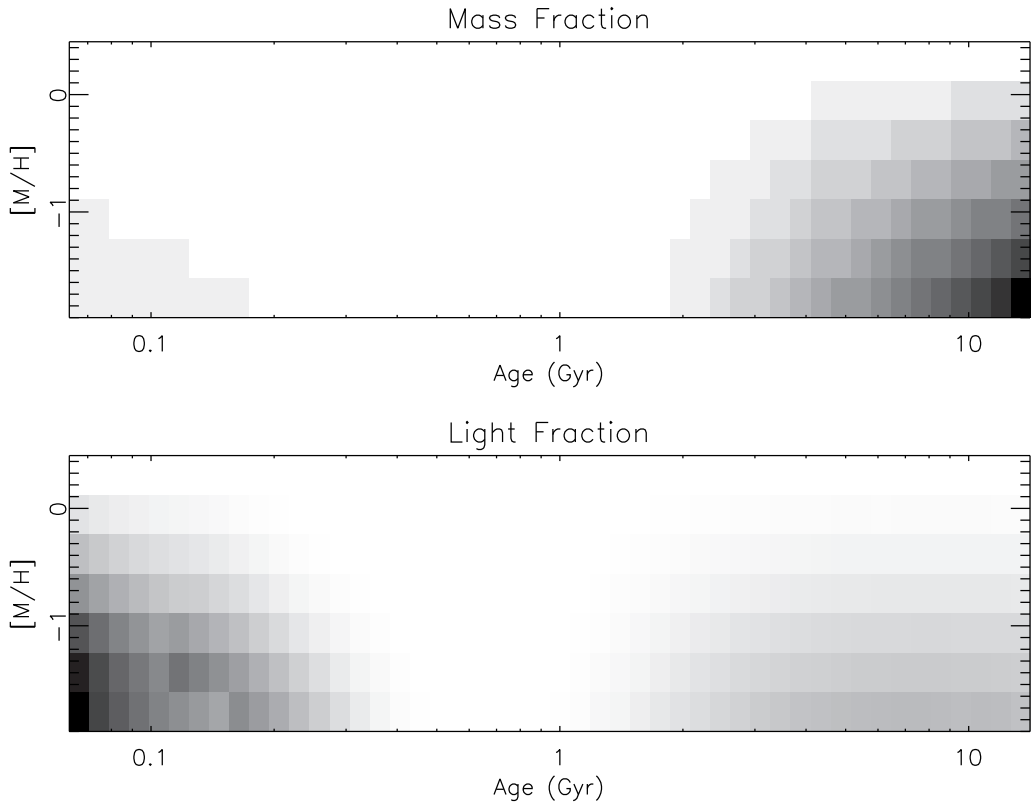

Supplementary Figure 10 | Relative mass and light fractions of stellar populations in Gal2 with respect to metallicity and age, suggesting the presence of young stellar populations of $\lesssim$0.3 Gyr.

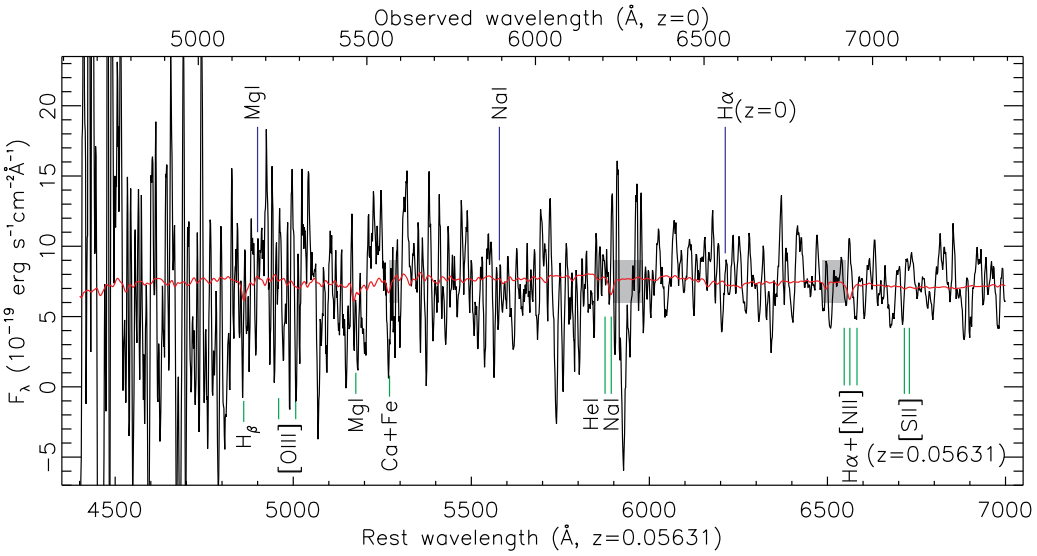

Supplementary Figure 11 | The pPXF fit to the Gemini spectrum of the counterpart to J2150−0551, showing no significant emission lines or absorption features. We assume the spectrum to be blueshifted by 300 km s^{-1} relative to Gal1 in the pPXF fit. The expected typical AGN emission lines and stellar absorption features are also marked below the spectrum. We also mark the expected typical emission/absorption lines in the case that J2150−0551 is a Galactic object with zero redshift. The spectrum is noisy and has been smoothed with a box function of width 8.6Å (the FWHM resolution of the spectrum) for clarity. The gray areas mark some portions of the spectrum seriously affected by the atmospheric OH absorption and CCD gaps.

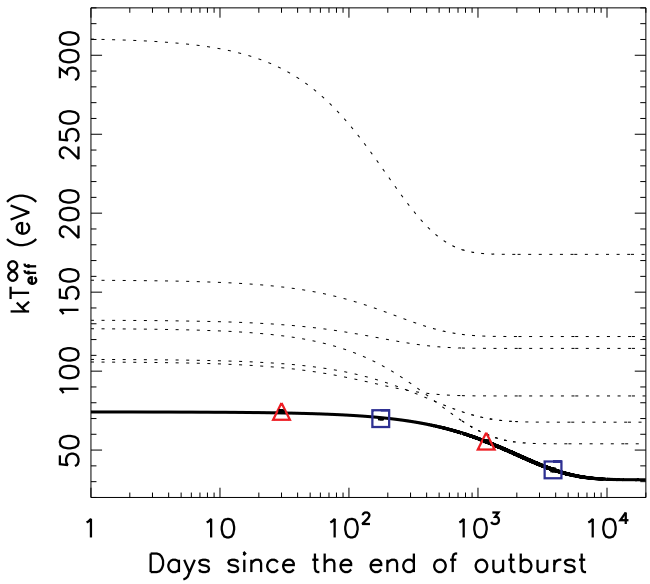

Supplementary Figure 12 | Evolution of the effective temperature based on the *nsatmos* fits to the X-ray spectra of J2150−0551, assuming an NS of mass 1.4 $M_{\odot}$ and radius 10 km. The error bars, smaller than the symbol size, are at the 90% confidence level. The dotted lines plot the fits of the cooling curves from six cooling NSs (MAXI J0556−332, XTE J1701−462, EXO 0748−676, MXB 1659−29, KS 1731−260, IGR J17480−2446, from the top to the bottom at the time of day 1)[51] with an exponential decay to a constant ($T_{\rm eff}^{\infty}(t) = T_1 \exp^{-t/\tau} + T_0$). For J2150−0551, the ending date of the hypothetical accretion outburst is unknown, and we assumed it to be one month before X1 when we fitted the cooling curve (solid line). The fit inferred a decaying timescale of 2008 days, which is independent of the ending date of the accretion outburst assumed.

64. Jones, D. H. *et al.* The 6dF Galaxy Survey: final redshift release (DR3) and southern large-scale structures. *Mon. Not. R. Astron. Soc.* **399**, 683–698 (2009). 0903.5451.
65. Skrutskie, M. F. *et al.* The Two Micron All Sky Survey (2MASS). *Astron. J.* **131**, 1163–1183 (2006).
66. Larsen, S. S. Young massive star clusters in nearby galaxies. II. Software tools, data reductions and cluster sizes. *Astron. Astrophys. Suppl.* **139**, 393–415 (1999). astro-ph/9907163.
67. Arnaud, K. A. XSPEC: The First Ten Years. In Jacoby, G. H. & Barnes, J. (eds.) *Astronomical Data Analysis Software and Systems V*, vol. 101 of *Astronomical Society of the Pacific Conference Series*, 17–+ (1996).
68. Kalberla, P. M. W. *et al.* The Leiden/Argentine/Bonn (LAB) Survey of Galactic HI. Final data release of the combined LDS and IAR surveys with improved stray-radiation corrections. *Astron. Astrophys.* **440**, 775–782 (2005). arXiv:astro-ph/0504140.
69. Wilms, J., Allen, A. & McCray, R. On the Absorption of X-Rays in the Interstellar Medium. *Astrophys. J.* **542**, 914–924 (2000). astro-ph/0008425.
70. Katz, J. I. Acceleration, radiation and precession in SS 433. *Astrophys. J.* **236**, L127–L130 (1980).
71. Abramowicz, M. A., Czerny, B., Lasota, J. P. & Szuszkiewicz, E. Slim accretion disks. *Astrophys. J.* **332**, 646–658 (1988).
72. Fukue, J. Critical Accretion Disk. *Publ. Astron. Soc. Japan* **56**, 569–580 (2004).
73. Ohsuga, K. & Mineshige, S. Why Is Supercritical Disk Accretion Feasible? *Astrophys. J.* **670**, 1283–1290 (2007). arXiv:0710.2941.
74. Lin, D., Remillard, R. A. & Homan, J. Spectral States of XTE J1701-462: Link Between Z and Atoll Sources. *Astrophys. J.* **696**, 1257–1277 (2009). 0901.0031.
75. Heinke, C. O., Rybicki, G. B., Narayan, R. & Grindlay, J. E. A Hydrogen Atmosphere Spectral Model Applied to the Neutron Star X7 in the Globular Cluster 47 Tucanae. *Astrophys. J.* **644**, 1090–1103 (2006). astro-ph/0506563.
76. Zavlin, V. E., Pavlov, G. G. & Shibanov, Y. A. Model neutron star atmospheres with low magnetic fields. I. Atmospheres in radiative equilibrium. *Astron. Astrophys.* **315**, 141–152 (1996). astro-ph/9604072.
77. Gierliński, M., Done, C. & Page, K. Reprocessing of X-rays in the outer accretion disc of the black hole binary XTE J1817-330. *Mon. Not. R. Astron. Soc.* **392**, 1106–1114 (2009). 0808.4064.
78. Lamastra, A. *et al.* The bolometric luminosity of type 2 AGN from extinction-corrected [OIII]. No evidence of Eddington-limited sources. *Astron. Astrophys.* **504**, 73–79 (2009). 0905.4439.
79. Komossa, S. Ludwig Biermann Award Lecture: X-ray Evidence for Supermassive Black Holes at the Centers of Nearby, Non-Active Galaxies. In R. E. Schielicke (ed.) *Reviews in Modern Astronomy*, vol. 15, 27–+ (2002). arXiv:astro-ph/0209007.
80. Lin, D. *et al.* Discovery of an Ultrasoft X-Ray Transient Source in the 2XMM Catalog: A Tidal Disruption Event Candidate. *Astrophys. J.* **738**, 52–+ (2011). 1106.0744.
81. Lin, D. *et al.* An Ultrasoft X-Ray Flare from 3XMM J152130.7+074916: A Tidal Disruption Event Candidate. *Astrophys. J.* **811**, 43 (2015). 1509.00840.
82. Miller, M. C. Disk Winds as an Explanation for Slowly Evolving Temperatures in Tidal Disruption Events. *Astrophys. J.* **805**, 83 (2015). 1502.03284.
83. Makishima, K. *et al.* Simultaneous X-ray and optical observations of GX 339-4 in an X-ray high state. *Astrophys. J.* **308**, 635–643 (1986).
84. Shakura, N. I. & Sunyaev, R. A. Black holes in binary systems. Observational appearance. *Astron. Astrophys.* **24**, 337–355 (1973).
85. Israel, G. L. *et al.* An accreting pulsar with extreme properties drives an ultraluminous x-ray source in NGC 5907. *Science* **355**, 817–819 (2017). 1609.07375.
86. Walton, D. J. *et al.* Super-Eddington accretion on to the neutron star NGC 7793 P13: Broad-band X-ray spectroscopy and ultraluminous X-ray sources. *Mon. Not. R. Astron. Soc.* **473**, 4360–4376 (2018). 1705.10297.
87. Komossa, S. Tidal disruption of stars by supermassive black holes: Status of observations. *JHEA* **7**, 148–157 (2015). 1505.01093.
88. Hung, T. *et al.* Revisiting Optical Tidal Disruption Events with iPTF16axa. *Astrophys. J.* **842**, 29 (2017). 1703.01299.
89. Stone, N., Sari, R. & Loeb, A. Consequences of strong compression in tidal disruption events. *Mon. Not. R. Astron. Soc.* **435**, 1809–1824 (2013). 1210.3374.
90. Hilker, M., Infante, L., Vieira, G., Kissler-Patig, M. & Richtler, T. The central region of the Fornax cluster. II. Spectroscopy and radial velocities of member and background galaxies. *Astronomy & Astrophysics Supplement* **134**, 75–86 (1999). astro-ph/9807144.
91. Drinkwater, M. J., Jones, J. B., Gregg, M. D. & Phillipps, S. Compact Stellar Systems in the Fornax Cluster: Super-massive Star Clusters or Extremely Compact Dwarf Galaxies? *PASA* **17**, 227–233 (2000). astro-ph/0002003.
92. Phillipps, S., Drinkwater, M. J., Gregg, M. D. & Jones, J. B. Ultracompact Dwarf Galaxies in the Fornax Cluster. *Astrophys. J.* **560**, 201–206 (2001). astro-ph/0106377.
93. Bellovary, J. M. *et al.* Wandering Black Holes in Bright Disk Galaxy Halos. *Astrophys. J.* **721**, L148–L152 (2010). 1008.5147.
94. Jennings, Z. G. *et al.* NGC 3628-UCD1: A Possible ω Cen Analog Embedded in a Stellar Stream. *Astrophys. J.* **812**, L10 (2015). 1509.04710.
95. Arcavi, I. *et al.* A Continuum of H- to He-rich Tidal Disruption Candidates With a Preference for E+A Galaxies. *Astrophys. J.* **793**, 38 (2014). 1405.1415.
96. Vinkó, J. *et al.* A Luminous, Fast Rising UV-transient Discovered by ROTSE: A Tidal Disruption Event? *Astrophys. J.* **798**, 12 (2015). 1410.6014.
97. Arcavi, I. *et al.* Rapidly Rising Transients in the Supernova-Superluminous Supernova Gap. *Astrophys. J.* **819**, 35 (2016). 1511.00704.
98. Auchettl, K., Guillochon, J. & Ramirez-Ruiz, E. New Physical Insights about Tidal Disruption Events from a Comprehensive Observational Inventory at X-Ray Wavelengths. *Astrophys. J.* **838**, 149 (2017). 1611.02291.
99. Reines, A. E. & Comastri, A. Observational Signatures of High-Redshift Quasars and Local Relics of Black Hole Seeds. *PASA* **33**, e054 (2016). 1609.03562.
100. Kaaret, P., Feng, H. & Roberts, T. P. Ultraluminous X-Ray Sources. *Annu. Rev. Astron. Astrophys.* **55**, 303–341 (2017). 1703.10728.
101. Mezcua, M. Observational evidence for intermediate-mass black holes. *International Journal of Modern Physics D* **26**, 1730021 (2017). 1705.09667.
102. Gebhardt, K., Rich, R. M. & Ho, L. C. An Intermediate-Mass Black Hole in the Globular Cluster G1: Improved Significance from New Keck and Hubble Space Telescope Observations. *Astrophys. J.* **634**, 1093–1102 (2005). astro-ph/0508251.
103. Webb, N. *et al.* Radio Detections During Two State Transitions of the Intermediate-Mass Black Hole HLX-1. *Science* **337**, 554– (2012).
104. Lützgendorf, N. *et al.* Limits on intermediate-mass black holes in six Galactic globular clusters with integral-field spectroscopy. *Astron. Astrophys.* **552**, A49 (2013). 1212.3475.
105. Pasham, D. R., Strohmayer, T. E. & Mushotzky, R. F. A 400-solar-mass black hole in the galaxy M82. *Nature* **513**, 74–76 (2014).
106. Lützgendorf, N. *et al.* Re-evaluation of the central velocity-dispersion profile in NGC 6388. *Astron. Astrophys.* **581**, A1 (2015). 1507.02813.
107. Mezcua, M., Roberts, T. P., Lobanov, A. P. & Sutton, A. D. The powerful jet of an off-nuclear intermediate-mass black hole in the spiral galaxy NGC 2276. *Mon. Not. R. Astron. Soc.* **448**, 1893–1899 (2015). 1501.04897.
108. Barth, A. J., Ho, L. C., Rutledge, R. E. & Sargent, W. L. W. POX 52: A Dwarf Seyfert 1 Galaxy with an Intermediate-Mass Black Hole. *Astrophys. J.* **607**, 90–102 (2004). astro-ph/0402110.
109. Ho, L. C., Kim, M. & Terashima, Y. The Low-mass, Highly Accreting Black Hole Associated with the Active Galactic Nucleus 2XMM J123103.2+110648. *Astrophys. J.* **759**, L16 (2012). 1210.0440.
110. Maksym, W. P., Lin, D. & Irwin, J. A. RBS 1032: A Tidal Disruption Event in Another Dwarf Galaxy? *Astrophys. J.* **792**, L29 (2014). 1407.2928.
111. Maksym, W. P. *et al.* Deep spectroscopy of the MV -14.8 host galaxy of a tidal disruption flare in A1795. *Mon. Not. R. Astron. Soc.* **444**, 866–873 (2014). 1407.6737.
112. Baldassare, V. F., Reines, A. E., Gallo, E. & Greene, J. E. A 50,000 Solar Mass Black Hole in the Nucleus of RGG 118. *Astrophys. J.* **809**, L14 (2015). 1506.07531.
113. Maksym, W. P., Ulmer, M. P., Eracleous, M. C., Guennou, L. & Ho, L. C. A tidal flare candidate in Abell 1795. *Mon. Not. R. Astron. Soc.* **435**, 1904–1927 (2013). 1307.6556.
114. Lin, D., Webb, N. A. & Barret, D. Classification of X-Ray Sources in the XMM-Newton Serendipitous Source Catalog. *Astrophys. J.* **756**, 27 (2012). 1207.1913.
115. Lin, D., Irwin, J. A., Godet, O., Webb, N. A. & Barret, D. A ˜ 3.8 hr Periodicity from an Ultrasoft Active Galactic Nucleus Candidate. *Astrophys. J.* **776**, L10 (2013). 1309.4440.
116. Lin, D., Webb, N. A. & Barret, D. Classification of X-Ray Sources in the XMM-Newton Serendipitous Source Catalog: Objects of Special Interest. *Astrophys. J.* **780**, 39 (2014). 1309.0509.

117. Terashima, Y., Kamizasa, N., Awaki, H., Kubota, A. & Ueda, Y. A Candidate Active Galactic Nucleus with a Pure Soft Thermal X-Ray Spectrum. *Astrophys. J.* **752**, 154 (2012). 1205.2774.
118. Miniutti, G. *et al.* A high Eddington-ratio, true Seyfert 2 galaxy candidate: implications for broad-line region models. *Mon. Not. R. Astron. Soc.* **433**, 1764–1777 (2013). 1305.3284.
119. Plotkin, R. M. *et al.* The 2015 Decay of the Black Hole X-Ray Binary V404 Cygni: Robust Disk-jet Coupling and a Sharp Transition into Quiescence. *Astrophys. J.* **834**, 104 (2017). 1611.02810.
120. Kahabka, P. & van den Heuvel, E. P. J. *Super-soft sources*, 461–474 (2006).
121. Dupuy, T. J. & Liu, M. C. The Hawaii Infrared Parallax Program. I. Ultracool Binaries and the L/T Transition. *Astrophys. J. Suppl. Ser.* **201**, 19 (2012). 1201.2465.
122. Wijnands, R. *et al.* The XMM-Newton/Chandra monitoring campaign of the Galactic center region. Description of the program and preliminary results. *Astron. Astrophys.* **449**, 1117–1127 (2006). arXiv:astro-ph/0508648.
123. Degenaar, N. & Wijnands, R. The behavior of subluminous X-ray transients near the Galactic center as observed using the X-ray telescope aboard Swift. *Astron. Astrophys.* **495**, 547–559 (2009). 0807.3458.
124. Campana, S. Linking Burst-Only X-Ray Binary Sources to Faint X-Ray Transients. *Astrophys. J.* **699**, 1144–1152 (2009). 0905.0607.
125. Heinke, C. O., Bahramian, A., Degenaar, N. & Wijnands, R. The nature of very faint X-ray binaries: hints from light curves. *Mon. Not. R. Astron. Soc.* **447**, 3034–3043 (2015). 1412.4097.
126. Ootes, L. S., Page, D., Wijnands, R. & Degenaar, N. Neutron star crust cooling in KS 1731-260: the influence of accretion outburst variability on the crustal temperature evolution. *Mon. Not. R. Astron. Soc.* **461**, 4400–4405 (2016). 1606.01923.
127. Merritt, R. L. *et al.* The Thermal State of KS 1731-260 after 14.5 years in Quiescence. *Astrophys. J.* **833**, 186 (2016). 1608.03880.
128. Waterhouse, A. C. *et al.* Constraining the properties of neutron star crusts with the transient low-mass X-ray binary Aql X-1. *Mon. Not. R. Astron. Soc.* **456**, 4001–4014 (2016). 1512.06129.
129. Parikh, A. S. *et al.* Different accretion heating of the neutron star crust during multiple outbursts in MAXI J0556-332. *ArXiv e-prints* (2017). 1710.09365.
130. Fridriksson, J. K. *et al.* The Variable Quiescent X-Ray Emission of the Transient Neutron Star XTE J1701-462. *Astrophys. J.* **736**, 162 (2011). 1101.0081.
131. Fialkov, A. & Loeb, A. Jetted tidal disruptions of stars as a flag of intermediate mass black holes at high redshifts. *Mon. Not. R. Astron. Soc.* **471**, 4286–4299 (2017). 1611.01386.
132. Rosen, S. R. *et al.* The XMM-Newton serendipitous survey. VII. The third XMM-Newton serendipitous source catalogue. *Astron. Astrophys.* **590**, A1 (2016).
133. Wang, J. & Merritt, D. Revised Rates of Stellar Disruption in Galactic Nuclei. *Astrophys. J.* **600**, 149–161 (2004). astro-ph/0305493.
134. Kochanek, C. S. Tidal disruption event demographics. *Mon. Not. R. Astron. Soc.* **461**, 371–384 (2016). 1601.06787.
135. Pfeffer, J., Griffen, B. F., Baumgardt, H. & Hilker, M. Contribution of stripped nuclear clusters to globular cluster and ultracompact dwarf galaxy populations. *Mon. Not. R. Astron. Soc.* **444**, 3670–3683 (2014). 1408.4467.
136. Murray, S. G., Power, C. & Robotham, A. S. G. HMFcalc: An online tool for calculating dark matter halo mass functions. *Astronomy and Computing* **3**, 23–34 (2013). 1306.6721.